Nuclear interaction model with explicit mesons and relativistic kinetic energy

Kerneinteraktionsmodel med eksplicitte mesoner og relativistisk kinetisk energi

Jakob Rye
201303684 – au460980
Aarhus University
Department of Physics and Astronomy

Master Thesis

Date: 1TH of September, 2023
Supervisor: D. V. Fedorov

Abstract

The nuclear model with explicit mesons has been proposed to describe the strong interaction between nucleons. In the explicit meson model the mesons are treated explicitly as an degree of freedom. In the model the nucleus becomes a superposition of states with differing numbers of emitted mesons. The state transitions allow bound nuclear states. The simplest incarnation of the model is the one-meson approximation with the sigma-meson, and this incarnation can be applied to the deuteron.

By using a coupling between states proposed by D. V. Fedorov the model is able to produce acceptable values for the ground state energy and charge radius for a deuteron. Hence, confirming the result the previous examination. Applying the coupling proposed by Filip Jensen to the deuteron the model produces bound states, however the produced ground state energy and charge radius do not have acceptable values. This result also confirms previous findings. By including the interaction between single nucleons and mesons into the model with Filip Jensen's coupling, the model is able to produce acceptable results.

The contribution from higher order approximations and the correction from relativistic kinetic energy are examined for different meson masses. The results imply that future studies that include the pion into the explicit meson model should use the relativistic kinetic energy.

With the success of the explicit meson model on a deuteron system future studies can take on more complex systems.

Acknowledgements

I would like to thank my supervisor, D. V. Fedorov, for his support and patience during the elaboration of this thesis. He has been open to discussing a variety of relevant subjects and feedback. He has also borrowed me relevant material and offered useful advice for which I am very grateful.

I would like to thank my family for their support and for letting me borrow their summer cottage during the last phase of the writing.

Contents

1

Introduction

One of the fundamental interactions of nature is the strong interaction between nucleons. In the low energy regime the strong interaction is believed to be mediated by mesons [13]. Common methods for describing the strong interaction are One Boson Exchange Potential and Effective Field Theory. Inspired by the successes of these models the explicit meson model has been introduced [1][6].

The explicit meson model is a phenomenological model with mesons as explicit degrees of freedom. In this model the nucleus becomes a superposition of states with differing number of emitted mesons. The energy requirement of meson emission impose a potential barrier, proportional to the number of mesons, onto the states. Compared to other descriptions of the strong interaction the potential advantage of the explicit meson model is a reduced number of model parameters. The explicit meson model naturally includes few-body forces and meson physics.

So far only few studies have investigated the explicit meson model with sigma-mesons [1][6]. These studies have applied the model to the deuteron. Since the deuteron is the simplest stable nucleus, consisting of a proton and a neutron, it is a logical first choice for investigations of the validity of the explicit meson model. For a discussion of the s-wave part of the deuteron wave-function see [14]. The investigations of deuteron in [1][6] have shown different levels of success. These studies were limited by a simple approximation with one emitted sigma-meson. The studies have assumed that the kinetic energy for the deuteron system does not have a significant relativistic correction.

Pions have been incorporated into the explicit meson model in [5][8] to investigate photoproduction off protons. In [5][8] Fedorov and Mikkelsen have successfully reproduced the experimental cross section for neutral pion photoproduction off protons. These studies further encourage the development and investigation of the explicit meson model.

In this thesis the results from the previous studies, [1][6], of the explicit meson model will be recreated and expanded. The emission of mesons from single nucleons will be investigated, so the dressing of single nucleons can be incorporated into the model. The assumption of nonrelativistic kinetic energy will be tested by comparing the model with nonrelativistic and relativistic energy.

The thesis structure is as follows:

In Chapter 2 the notation used throughout the thesis is presented. Chapter 3 introduces Jacobi coordinate transformation. The explicit meson model is presented in Chapter 4.

Chapter 5 is an introduction of the variational method in quantum physics. In Chapter 6 the explicitly correlated Gaussian mehod used in the variational calculations is introduced along with relevant matrix elements. The non-analytic matrix element for the relativist kinetic energy is calculated in Chapter 7. Some numerical tools relevant to the results in later sections are presented in Chapter 8.

In Chapter 9 the results of previous examinations of the explicit meson model [1][6] are recreated.

Chapter 10 contains the results not previously examined. These include: Section 10.1 where the correction from meson-nucleon system is included in the explicit meson model and tested on a deuteron system, Section 10.2 where the correction from a second meson is investigated and Section 10.3 which contains a comparison between the relativistic and nonrelativistic model.

Chapter 11 contains the discussion of the results from the previous sections and Chapter 12 is the conclusion of this thesis.

2

Notation

This section introduces some notation used throughout this thesis following the convention set by [6]. Let $\mathbf{r}$ be the position vector for a system of N particles, with $\vec{r}_i$ being the 3-dimensional position vector for the i'th particle:

$$\mathbf{r} = \begin{pmatrix} \vec{r}_1 \\ \vdots \\ \vec{r}_N \end{pmatrix}. \tag{2.1}$$

If A is a $N \times N$ matrix then $A\mathbf{r}$ is given by:

$$(A\mathbf{r})_i = \sum_{j=1}^{N} A_{j,i}\vec{r}_j. \tag{2.2}$$

The product with a N-dimensional vector v is given by:

$$v^T\mathbf{r} = \sum_{i=1}^{N} v_i\vec{r}_i. \tag{2.3}$$

If A is a $N \times N$ matrix, then the reduced matrix $\lfloor A \rfloor$ is the $(N-1) \times (N-1)$ matrix where the N'th row and column have been removed from the A matrix. The same notation can be applied to vectors. The general N

dimensional vector $\mathbf{v} = (\vec{v}_1, \cdots, \vec{v}_N)^{\mathrm{T}}$ can be reduced to $\lfloor \mathbf{v} \rfloor$ by removing the last component $\vec{v}_N$.

A $N \times N$ matrix A can be expanded to a $(N+1) \times (N+1)$ matrix $\lceil A \rceil$ by adding a row and column of zeros:

$$\lceil A \rceil = \begin{pmatrix} A & \vec{0} \\ \vec{0}^T & 0 \end{pmatrix}, \tag{2.4}$$

where $\vec{0}$ is a zero vector of dimension N.

This notation gives rise to a pair of useful identities [6]:

$$\lfloor A\vec{v} \rfloor = \lfloor A \rfloor \lfloor \vec{v} \rfloor + v_N \lfloor \vec{a_N} \rfloor, \tag{2.5}$$

$$\lfloor \vec{v} \rfloor^T A \lfloor \vec{v} \rfloor = \vec{v}^T \lceil A \rceil \vec{v}, \tag{2.6}$$

where A is a $N \times N$ matrix with column vectors $(\vec{a_1}, \vec{a_2}, \cdots, \vec{a_N})$ and $\vec{v}$ is a vector of dimension N.

3

Coordinate transformation

The Jacobi (Center-of-mass) coordinate transformation allows the elimination of the center-of-mass motion, hence simplifying the numerical calculations.

The coordinate center-of-mass transformation from $\mathbf{r}$ to the Jacobi coordinates $\mathbf{x}$:

$$\mathbf{r} \rightarrow \mathbf{x} = J\mathbf{r}, \tag{3.1}$$

where J is the transformation matrix.

The transformation matrix J for a system of N particle is given as:

$$J_{k,j} = \begin{cases} \frac{m_j}{\sum_{i=1}^{k} m_i} & \text{for } j \leq k \\ -1 & \text{for } j = k+1 \\ 0 & \text{else} \end{cases}, \tag{3.2}$$

where $m_1, m_2, \cdots, m_N$ are the masses associated with the system.

The classical kinetic energy matrix transforms as:

$$K \rightarrow JKJ^T. \tag{3.3}$$

A description of the coordinate transformation of relativistic kinetic energy is given in Chapter 7. Cyclic permutations of the Jacobi transformation is discussed in Appendix A.

4

The explicit meson model

In this section the explicit meson model is introduced with respect to a deuteron system. A deuteron is a simple nucleus consisting of two nucleons, a neutron and a proton. Hence, a deuteron system presents a natural first trial of the explicit meson model.

In the low energy regime the nucleon-nucleon interaction is believed to be mediated by mesons [14]. The explicit meson model allows nucleons to explicitly emit and absorb mesons. In the model the mesons are treated in the same manor as the nucleons. Consequently the nucleus becomes a superposition of states with differing numbers of emitted mesons. For the deuteron system the Hamiltonian is given by the matrix [6]:

$$H = \begin{pmatrix} K_N & W & 0 & \\ W & K_N + K_\sigma + m_\sigma & W & \cdots \\ 0 & W & K_N + K_{2\sigma} + 2m_\sigma & \\ & \vdots & & \ddots \end{pmatrix} \tag{4.1}$$

where K_N is the kinetic energy of the nucleons, K_σ is the kinetic energy of the meson, m_σ is the mass of the meson and W is coupling term between the subsystems. In the low energy-regime the states with emitted mesons are under a potential barrier due to the energy required for the generation of mesons. The strength of the potential is equal to the total mass of the mesons for a given state.

It should be noted that zero energy is set equal to the total mass of the nucleons $m_n + m_p$, where m_p is the proton mass and m_n is the neutron

mass. This simplifies the model to the form in Eq. (4.1), and this must be kept in mind when incorporating dressed states into the model.

The Schrödinger equation corresponding to the Hamiltonian is:

$$H\left|\Psi\right\rangle = E_0\left|\Psi\right\rangle, \tag{4.2}$$

where the wave-function $|\Psi\rangle$ is a linear combination with a component for every row in the Hamiltonian:

$$\left|\Psi\right\rangle = \begin{pmatrix} |\psi_N\rangle \\ |\psi_{N+\sigma}\rangle \\ \vdots \end{pmatrix}. \tag{4.3}$$

In this trial of the explicit meson model the only allowed meson is the scalar-isoscalar sigma-meson. The sigma-meson is believed to be responsible for the majority of the intermediate range interactions between nucleons.

4.1 Classical kinetic energy

For a N-body system consisting of particles with coordinates $\vec{r}_i$ a general form of the classical kinetic energy operator $\hat{K}$ is given as [2]:

$$\hat{K} = -\sum_{i,j=1}^{N} \frac{\partial}{\partial \vec{r}_i}\Lambda_{i,j}\frac{\partial}{\partial \vec{r}_j} \equiv \frac{\partial}{\partial \mathbf{r}}\Lambda\frac{\partial}{\partial \mathbf{r}^{\mathrm{T}}}, \tag{4.4}$$

where Λ is a symmetric positive-defined matrix.

The relativistic kinetic energy is described in Chapter 7.

4.2 One-meson approximation

In the explicit meson model the states with mesons find themselves under a potential barrier equal to the total mass of the mesons. The expectation is that in the first approximation only the state with one meson will have a significant contribution to the system [1]. This subsection presents the one-meson approximation in some detail, due to its significance to later

discussions. Higher order approximations, such as the two-meson approximation, follow naturally as a generalization of the one-meson approximation.

The Hamiltonian for the nucleus in the one-meson approximation becomes a 2×2 matrix:

$$H = \begin{pmatrix} K_N & W \\ W & K_N + K_\sigma + m_\sigma \end{pmatrix}. \tag{4.5}$$

The corresponding Schrödinger equation is then given as:

$$\begin{pmatrix} K_N & W \\ W & K_N + K_\sigma + m_\sigma \end{pmatrix} \begin{pmatrix} \psi_N \\ \psi_{N\sigma} \end{pmatrix} = E_0 \begin{pmatrix} \psi_N \\ \psi_{N\sigma} \end{pmatrix}, \tag{4.6}$$

where ψ_N is the wave-function of the subsystem consisting of nucleons without any mesons and $\psi_{N\sigma}$ is the wave-function of the subsystem consisting of nucleons and a meson. If the energy E_0 is higher than the meson mass the potential prevents the meson from leaving the nucleus.

A deuteron system consists of a proton and a neutron, hence the wave-function in the one-meson approximation becomes a superposition of a two-body subsystem and a three-body subsystem. The center-of-mass coordinate for the two-body subsystem is:

$$\mathbf{r}_{(d)} = \left(\vec{r}_{np}\right), \tag{4.7}$$

where $\vec{r}_{np}$ is the first coordinate in the Jacobi transformation given in Eq. (3.2). The reduced mass for the two-body subsystem is:

$$\mu_{np} = \frac{m_n m_p}{m_n + m_p}, \tag{4.8}$$

where m_n is the neutron mass and m_p is the proton mass.

In the two-body subsystem the Λ matrix in Eq. (4.4) is:

$$\Lambda_{(d)} = \left(\frac{\hbar^2}{2\mu_{np}}\right). \tag{4.9}$$

The center-of-mass coordinate for the three-body subsystem consisting of a proton, a neutron and a meson has two components:

$$\mathbf{r}_{(\sigma)} = \begin{pmatrix} \vec{r}_{np} \\ \vec{r}_{\sigma np} \end{pmatrix}. \tag{4.10}$$

The reduced mass of the three-body susystem becomes:

$$\mu_{\sigma np} = \frac{m_\sigma (m_n + m_p)}{m_\sigma + m_n + m_p}, \tag{4.11}$$

where m_σ is the mass of the sigma-meson. For the three-body system the Λ matrix in Eq. (4.4) is:

$$\Lambda_{(\sigma)} = \begin{pmatrix} \frac{\hbar^2}{2\mu_{np}} & 0 \\ 0 & \frac{\hbar^2}{2\mu_{\sigma np}} \end{pmatrix}. \tag{4.12}$$

4.3 Coupling term

In Eq. (4.1) the term W is the coupling between states with a differing number of mesons. Previous studies of the explicit meson model [1] [6] have proposed different coupling terms. This section will describe different coupling terms and show their form in the one-meson approximation.

In a realistic model the individual nucleon is allowed to emit mesons. This is a feature of the coupling proposed by Filip Jensen in Eq. (4.16) [6]. For the general case with s sigma-mesons and $N = s + 2$ particles the coupling term for the proton is given by [6]:

$$\left\langle \mathbf{r}' \middle| \mathcal{G}_{p,\mathcal{P}} \middle| \mathbf{r} \right\rangle = \delta^{3N} \left(\mathbf{r} - \left\lfloor P\mathbf{r}' \right\rfloor \right) \frac{1}{\gamma\sqrt{\pi}} \mathrm{e}^{-\frac{1}{\gamma^2}\left(\vec{r}_p - (P\mathbf{r}')_{N+1}\right)^2}, \tag{4.13}$$

where P is the permutation operator for the sigma-mesons corresponding to the permutation $\mathcal{P}$, $\vec{r}_p$ is the position coordinate for the proton and γ is a range parameter with units of length.

The coupling term for the neutron $\mathcal{G}_{n,\mathcal{P}}$ has the same form as Eq. (4.14), where the position coordinate for the proton is replaced with the position

coordinate for the neutron $\vec{r}_p \to \vec{r}_n$. The full interaction is the sum of the contribution from the two nucleons [6]:

$$W_{FJ} = g \sum_{\mathcal{P}} \mathcal{G}_{p,\mathcal{P}} + \mathcal{G}_{n,\mathcal{P}}, \tag{4.14}$$

where the sum goes over every permutation of the mesons and g is the strength parameter.

In the one-meson approximation the permutation operator becomes the identity operator. By letting the strength parameter absorb the front factor Eq. (4.14) takes the form:

$$\left\langle \mathbf{r}_{(\sigma)} \middle| W_{FJ} \middle| \mathbf{r}_{(d)} \right\rangle = g' \left(\exp\left(-\frac{\vec{r}^2_{\sigma p}}{\gamma^2} \right) + \exp\left(-\frac{\vec{r}^2_{\sigma n}}{\gamma^2} \right) \right), \tag{4.15}$$

where $\vec{r}_{\sigma p} = \vec{r}_\sigma - \vec{r}_p$ and $\vec{r}_{\sigma n} = \vec{r}_\sigma - \vec{r}_n$ can be calculated using permutations of the coordinate transformation (see Eq. (7.10)).

This form of the coupling allows for bound states between single nucleons, hence the nucleons becomes "dressed" by the meson. In a realistic model the energy difference from dressed nucleon must be included into the model.

In [1] D. V. Fedorov's proposed a different coupling term in the one-meson approximation. This coupling assumes that the nucleons already are "dressed" with mesons, hence the operator only accounts for mesons emitted due to the presence of another nucleon. The coupling is given as:

$$\left\langle \mathbf{r}_{(\sigma)} \middle| W_{DF} \middle| \mathbf{r}_{(d)} \right\rangle = S_\sigma \exp\left(-\frac{\vec{r}^2_{np} + \vec{r}^2_{\sigma np}}{b^2_\sigma} \right), \tag{4.16}$$

where S_σ and b_σ are the strength and range parameter of the model respectively. It is assumed that the position of the nucleons remains fixed under the generation of the meson, hence the two-body and three-body systems share the same first coordinate. The coupling term in Eq. (4.16) goes to zero unless the three particles are in close proximity.

4.4 Charge radius

In addition to the state energies, the mean square charge radius is a property of nuclei that allows for a quantitative comparison between theoretical calculations and experimental data. For a system with N particles, the charge radius R_c can be defined as [1][7]:

$$R_c^2 = \sum_{i=1}^{N} Z_i \left\langle \vec{r}_i^{\,2} \right\rangle = \sum_{i=1}^{N} Z_i \left\langle \mathbf{r}^{\mathrm{T}} w_i w_i^{\mathrm{T}} \mathbf{r} \right\rangle , \tag{4.17}$$

where Z_i is the charge in unit charges of the i'th particle in the system, the brakets $\langle\rangle$ signify the expectation value in the given state of the system, $\vec{r}_i$ is the coordinate vector for the i'th particle of the system in the center-of-mass frame. w_i is the column unit vector for the i'th coordinate in the center-of-mass frame, hence $\vec{r}_i = w_i^{\mathrm{T}} \mathbf{r}$. Under the Jacobi coordinate transformation w_i transforms as $w_i \to J^{-\mathrm{T}} w_i$ (see Chapter 3).

In this model the only allowed meson in the explicit meson model is the chargeless sigma-meson, hence the only charge particle in the deuteron system is the proton. To compute the charge radius it is therefore sufficient to calculate the expectation value of the proton in Eq. (4.17).

5

Variational method

The variational method serves as the basis for a number of approaches for solving few-body problems in quantum physics, among them is the correlated Gaussian method used in this thesis [13]. Variational methods do not yield an exact solution, but given the right trial functions they can give a good approximation of the wave-function and ground state energy.

For a Hamiltonian H with associated ground-state energy E_0 the solution to the eigenvalue problem:

$$H\left|\tilde{\Psi}\right\rangle = E'\left|\tilde{\Psi}\right\rangle, \tag{5.1}$$

for any linear combination of trial functions $\left|\tilde{\Psi}\right\rangle = \sum_{i=1}^{m} c_i \left|\tilde{\psi}_i\right\rangle$, is a upper bound for the ground state energy $E' \geq E_0$ [12]. If the calculated upper limit for the energy approximates the ground state energy, it implies that the trial functions are a good approximation of the actual wave-function [12].

Multiplying Eq. (5.1) by $\left\langle\tilde{\psi}_j\right|$ to the left yields the generalized eigenvalue problem:

$$\mathcal{H}c = E'\mathcal{N}c, \tag{5.2}$$

where $\vec{c} = \{c_i\}$ is a vector of the linear parameters, the overlap matrix $\mathcal{N}$ and Hamiltonian matrix $\mathcal{H}$ are given as:

$$\mathcal{N}_{i,j} = \langle \tilde{\psi}_i | \tilde{\psi}_j \rangle \,, \tag{5.3}$$

$$\mathcal{H}_{i,j} = \langle \tilde{\psi}_i | H | \tilde{\psi}_j \rangle \,. \tag{5.4}$$

Solving the generalized eigenvalue problem yield the linear parameters $\vec{c} = \{c_i\}$.

The correlated Gaussian method described in Chapter 6 introduces a convenient set of trial functions that leads to analytic matrix elements for $\mathcal{N}$ and $\mathcal{H}$.

6

Correlated Gaussians method

A popular variational method for solving quantum-mechanical few-body problems such as evaluating the deuteron system in this thesis is the correlated Gaussian method (or explicitly correlated Gaussian method). The advantages of this method are that a number of relevant matrix elements are fully analytic, and thus simplifying the numerical calculation. In this section the correlated Gausians method is described and the relevant matrix elements are presented.

The variational method, described in Chapter 5, requires a reasonable set of trial functions. In the correlated Gaussian method a linear combination of stochastic generated Gaussian functions are chosen as the trial functions. In a system of N particles with coordinates $\mathbf{r}$, the correlated Gaussians have the form [2]:

$$\langle \mathbf{r}|A\rangle = \exp\left(-\sum_{i<j=1}^{N}\left(\frac{\vec{r}_i-\vec{r}_j}{b_{i,j}}\right)^2\right) \equiv \exp\left(-\mathbf{r}^{\mathrm{T}}A\mathbf{r}\right), \tag{6.1}$$

where $\vec{r}_i$ is the coordinate corresponding to the i-th particle, $b_{i,j}$ is the stochastic range parameter and the matrix A is given as:

$$A = \sum_{i<j=1}^{N}\frac{w_{i,j}w_{i,j}^{\mathrm{T}}}{b_{i,j}^2}, \tag{6.2}$$

where the vectors $w_{i,j}$ are defined through the equation:

$$\vec{r}_i - \vec{r}_j = w_{i,j}^{\mathrm{T}} \mathbf{r}. \tag{6.3}$$

In a two-body system in the laboratory frame $w_{i,j}$ is given as:

$$w_{1,2} = \begin{pmatrix} 1 \\ -1 \end{pmatrix}, \tag{6.4}$$

and for a three-body system the vectors are given as:

$$w_{1,2} = \begin{pmatrix} 1 \\ -1 \\ 0 \end{pmatrix}, \quad w_{1,3} = \begin{pmatrix} 1 \\ 0 \\ -1 \end{pmatrix}, \quad w_{2,3} = \begin{pmatrix} 0 \\ 1 \\ -1 \end{pmatrix}. \tag{6.5}$$

A given coordinate transformation $\mathbf{r} \to J\mathbf{r}$, $w_{i,j}$ transforms as $w_{i,j} \to \left(J^{-1}\right)^{\mathrm{T}} w_{i,j}$.

This thesis applies the correlate Gaussian method to the deuteron system described in the explicit meson model by the Hamiltonian in Eq. (4.1). The trial wave-function for the system is a linear combination of Gaussians with different dimensionality. For a given dimensionality d the trial function is:

$$|\tilde{\psi}_d\rangle = \sum_{i=1}^{n_d} c_{d,i} \, |A_{d,i}\rangle \,, \tag{6.6}$$

where n_d is the number of Gaussians with the given dimensionality. The full trial wave becomes:

$$\left|\tilde{\Psi}\right\rangle = \sum_d |\tilde{\psi}_d\rangle \,. \tag{6.7}$$

Returning to the generalized eigenvalue problem Eq. (5.2), the matrices $\mathcal{N}$ and $\mathcal{H}$ have a block structure:

$$\mathcal{H} = \begin{pmatrix} \langle A_{1,i}|K_N|A_{1,i'}\rangle & \langle A_{1,i}|W|A_{2,j}\rangle & \cdots \\ \langle A_{2,j}|W|A_{1,i}\rangle & \langle A_{2,j}|K_N + K_\sigma + m_\sigma|A_{2,j'}\rangle & \cdots \\ \vdots & \vdots & \ddots \end{pmatrix}, \tag{6.8}$$

$$\mathcal{N} = \begin{pmatrix} \langle A_{1,i}|A_{1,i'}\rangle & 0 & \cdots \\ 0 & \langle A_{2,j}|A_{2,j'}\rangle & \cdots \\ \vdots & \vdots & \ddots \end{pmatrix}, \tag{6.9}$$

where $i, i' = 1, \ldots, n_1$ and $j, j' = 1, \ldots, n_2$.

6.1 Overlap and classical kinetic energy

To evaluate the generalized eigenvalue problem in Eq. (5.2), the matrix elements in Eq. (5.3) must be computed. This subsection shows the matrix elements for the overlap and classical kinetic energy.

The overlap $\langle A'|A\rangle$ between two N-particle Gaussians $|A\rangle$ and $|A'\rangle$ is given as [2]:

$$\langle A'|A\rangle = \left(\frac{\pi^{(N-1)}}{\det(A + A')}\right)^{\frac{3}{2}}. \tag{6.10}$$

The general form of the classical kinetic energy operator $\hat{K}$ is given in Eq. (4.4). The corresponding matrix element is [2]:

$$\left\langle A' \middle| -\frac{\partial}{\partial \mathbf{r}} \Lambda \frac{\partial}{\partial \mathbf{r}^{\mathrm{T}}} \middle| A \right\rangle = 6\langle A'|A\rangle \mathrm{trace}\left(A'\Lambda A(A' + A)^{-1}\right). \tag{6.11}$$

6.2 Coupling term

In the explicit meson model the only allowed interaction between systems of different dimensions is through the coupling term. Hence, for all operators X, except the coupling term W [1]:

$$\left\langle A_{(m)} \middle| X \middle| A_{(m')} \right\rangle = 0, \tag{6.12}$$

where $\left|A_{(m)}\right\rangle$ and $\left|A_{(m')}\right\rangle$ are Gaussians with dimensionalities m and m' respectively, where $m, m' \in 1, 2, \cdots$ and $m \neq m'$.

If $m \in 1, 2, 3, \cdots$, then for any m-body Gaussian $A_{(m)}$ and $(m+1)$-body Gaussian $A_{(m-1)}$ the matrix element for the kernel in Eq. (4.13) is given as [6]:

$$\left\langle A_{(m)}\middle|\hat{\mathcal{G}}_{p,\mathcal{P}}\middle|A_{(m+1)}\right\rangle = \frac{1}{\gamma\sqrt{\pi}}\left(\frac{\pi^m}{\det\left(\mathcal{A}+A_{(m+1)}+\frac{\lfloor\omega_p\rfloor\lfloor\omega_p\rfloor^{\mathrm{T}}}{\gamma^2}\right)}\right)^{\frac{3}{2}}. \tag{6.13}$$

The matrix $\mathcal{A}$ is given by:

$$\mathcal{A} = \left\lfloor JPJ^{-1}\right\rfloor^{\mathrm{T}}\left\lceil A_{(m)}\right\rceil\left\lfloor JPJ^{-1}\right\rfloor, \tag{6.14}$$

where J is the coordinate transformation given in Eq. (3.2) and P is the permutation operator. In the one-meson approximation the permutation operator is unity, hence Eq. (6.14) becomes $\mathcal{A} = \left\lceil A_{(m)}\right\rceil$. The column vector ω_p is defined by:

$$\vec{\omega}_p = \left(PJ^{-1}\right)^{\mathrm{T}}\left(\mathbf{e}_p \check{} \mathbf{e}_{m+1}\right), \tag{6.15}$$

where $\mathbf{e}_p$ is the unit vector for the proton and $\mathbf{e}_{m+1}$ is the unit vector for the emitted meson. The last equality only holds true in the one-meson approximation, where $s = 0$.

The matrix element for $\hat{\mathcal{G}}_{n,\mathcal{P}}$ can be calculated using Eq. (6.13), by replacing $\mathbf{e}_p$ with the unit vector for the neutron $\mathbf{e}_n$ in Eq. (6.15).

So far the discussion of the coupling term has been for a arbitrary number of mesons. Continuing on with the one-meson approximation relevant for most of this thesis and discussion of the coupling term in Eq. (4.16). For a two-body Guassian $\left|A_{(d)}\right\rangle$ and a three-body Gaussian $\left|A_{(\sigma)}\right\rangle$ the matrix element of coupling term in Eq. (4.16) is [6]:

$$\left\langle A_{(d)}\middle|\hat{W}\middle|A_{(\sigma)}\right\rangle = S_\sigma\left\langle\tilde{A}\middle|A_{(\sigma)}\right\rangle, \tag{6.16}$$

where $\left|\tilde{A}\right\rangle$ is a Gaussian with associated 2×2 matrix $\tilde{A}$ given by:

$$\tilde{A} = \begin{pmatrix} A_{(d)} + \frac{1}{b_\sigma^2} & 0 \\ 0 & \frac{1}{b_\sigma^2} \end{pmatrix}. \tag{6.17}$$

6.3 Charge radius

The matrix element for the charge radius in Eq. (4.17) between two N-body Gaussians, $|A\rangle$ and $|A'\rangle$ is given as [2]:

$$\left\langle A \middle| \mathbf{r}^{\mathrm{T}} w_i w_i^{\mathrm{T}} \mathbf{r} \middle| A' \right\rangle = \frac{3}{2} w_i^{\mathrm{T}} \left(A + A'\right)^{-1} w_i \left\langle A \middle| A' \right\rangle. \tag{6.18}$$

7

Relativistic kinetic energy

For particles with high velocity the non-relativistic approximation for the kinetic energy no longer applies. The evaluations of the matrix element for relativistic kinetic energy in a correlate Gaussian basis are nontrivial. It turns out that the matrix element is non analytic. The matrix element for the relativistic kinetic energy is derived in this section following the approach from [13].

For a system of N particles the classical kinetic energy is given as:

$$T_{Cl} = \sum_{i=1}^{N} \frac{\vec{p}_i^2}{2m_i}, \tag{7.1}$$

where $\vec{p}_i$ and m_i is the momentum and mass of the i'th particle. The relativistic kinetic energy for the system is given by:

$$T_{SR} = \sum_{i=1}^{N} \sqrt{\vec{p}_i^2 + m_i^2} - m_i. \tag{7.2}$$

In Eq. (7.1) the center of mass motion can easily be separated. Eq. (4.4) gives the matrix element for the classical kinetic energy. The separation of the center of mass motion for the relativistic kinetic energy necessitates the introduction of permutations of the coordinate transformation. Permutations are discussed in more details in Appendix A. It turns out that the cyclic permutations of the coordinate transformation simplify the evaluation of the matrix element of $\sqrt{\vec{p}_i^2 + m_i^2}$.

7.1 Permutations of the coordinate transformation

Let J be the Jacobi coordinate transformation for a system of N particles, and let $P^{(k)}$ be the permutation operator for the k'th cyclic permutation of the system. Then the permutation of the coordinate transformation is given by:

$$J^{(k)} = P^{(k)} J. \tag{7.3}$$

For a three-particle system, such as a deuteron system in the one-meson approximation, the cyclic permutation of the coordinate transformation matrix is:

$$\begin{aligned} J^{(1)} &= \begin{pmatrix} 0 & 1 & -1 \\ -1 & \frac{m_2}{m_2+m_3} & \frac{m_3}{m_2+m_3} \\ \frac{m_1}{m_1+m_2+m_3} & \frac{m_2}{m_1+m_2+m_3} & \frac{m_3}{m_1+m_2+m_3} \end{pmatrix}, \\ J^{(2)} &= \begin{pmatrix} -1 & 0 & 1 \\ \frac{m_1}{m_1+m_3} & -1 & \frac{m_3}{m_1+m_3} \\ \frac{m_1}{m_1+m_2+m_3} & \frac{m_2}{m_1+m_2+m_3} & \frac{m_3}{m_1+m_2+m_3} \end{pmatrix}, \\ J^{(3)} &= J. \end{aligned} \tag{7.4}$$

Returning to the general N-particle system, the momentum of the i'th particle in the Jacobi coordinates is defined by the transformation:

$$\boldsymbol{\pi} \equiv J^{-1}\mathbf{p}, \tag{7.5}$$

where $\boldsymbol{\pi}$ is a size-N vector of particle momenta $\vec{\pi}_i$. Eq. (7.5) implies that the cyclic permutation of the momentum is:

$$\boldsymbol{\pi}^{(k)} = \left(J^{(k)}\right)^{-1} \mathbf{p}. \tag{7.6}$$

The motion of the system's center of mass is irrelevant to the internal mechanics of the system, hence the center of mass motion is set to zero:

$$\vec{\pi}_N \equiv \sum_{i=0}^{N} \vec{p}_i = 0. \tag{7.7}$$

Combining Eqs. (7.6) and (7.7) with the special form of the coordinate transformation matrix gives the useful substitution of the momentum into the center of mass frame:

$$\vec{p}_k = -\vec{\pi}_{N-1}^{(k)} \quad \text{for} \quad (k = 1, 2, \ldots, N). \tag{7.8}$$

This substitution can be inserted into the square root in Eq. (7.2):

$$\sqrt{\vec{p}_i^2 + m_i^2} = \sqrt{\left(\vec{\pi}_{N-1}^{(i)}\right)^2 + m_i^2}. \tag{7.9}$$

The transformation from the standard center of mass coordinates $\mathbf{x}$ to the permutation coordinates $\mathbf{x}^{(i)}$ is given by the matrix $V^{(i)}$:

$$\mathbf{x} = V^{(i)}\mathbf{x}^{(i)} \quad \text{with} \quad V^{(i)} = \left[J^{(N)} \left(J^{(i)}\right)^{-1} \right], \tag{7.10}$$

where $J^{(N)} = J$ follows from the definition of the permutations.

7.2 Calculating the matrix element

With the permutations of the coordinate transformation introduced, the matrix element of the relativistic kinetic energy can be evaluated. Let $|A\rangle$ and $|A'\rangle$ be $(N-1) \times (N-1)$ correlated Gaussians on the form given in Eq. (6.1). Applying Eq. (7.10) on the Gaussian $|A\rangle$ gives the useful relation:

$$\begin{aligned}
\langle \mathbf{x}|A\rangle &= \exp\left(-\mathbf{x}^{\mathrm{T}} A \mathbf{x}\right) \\
&= \exp\left(-\mathbf{x}^{\mathrm{T}} \left(V^{(i)}\right)^{-\mathrm{T}} \left(V^{(i)}\right)^{\mathrm{T}} A \left(V^{(i)}\right) \left(V^{(i)}\right)^{-1} \mathbf{x}\right) \\
&= \exp\left(-\left(\mathbf{x}^{(i)}\right)^{\mathrm{T}} A^{(i)} \mathbf{x}^{(i)}\right) \equiv \left\langle \mathbf{x}^{(i)} \middle| A^{(i)} \right\rangle,
\end{aligned} \tag{7.11}$$

where $A^{(i)} = (V^{(i)})^{\mathrm{T}} A V^{(i)}$.

Evaluating the matrix element $\sqrt{\vec{p}_i^2 + m_i^2}$ using Eqs. (7.10) and (7.11) gives the inner product:

$$\left\langle A' \middle| \sqrt{\vec{p}_i^2 + m_i^2} \middle| A \right\rangle = \left\langle A' \middle| \sqrt{\left(\vec{\pi}_{N-1}^{(i)}\right)^2 + m_i^2} \middle| A \right\rangle$$
$$= \left(\det V^{(i)}\right)^3$$
$$\times \int \mathrm{d}\mathbf{x}^{(i)} \left\langle A^{(i)\prime} \middle| \mathbf{x}^{(i)} \right\rangle \left\langle \mathbf{x}^{(i)} \middle| \sqrt{\left(\vec{\pi}_{N-1}^{(i)}\right)^2 + m_i^2} \middle| \mathbf{x}^{(i)} \right\rangle \left\langle \mathbf{x}^{(i)} \middle| A^{(i)} \right\rangle, \quad (7.12)$$

where $\left(\det V^{(i)}\right)^3$ is the Jacobian corresponding to the change of integration variable.

To further evaluate the integral in Eq. (7.12), the Fourier transformation can be applied to transition into momentum space:

$$\left(\det V^{(i)}\right)^3 \int \mathrm{d}\mathbf{x}^{(i)} \left\langle A^{(i)\prime} \middle| \mathbf{x}^{(i)} \right\rangle \left\langle \mathbf{x}^{(i)} \middle| \sqrt{\left(\vec{\pi}_{N-1}^{(i)}\right)^2 + m_i^2} \middle| \mathbf{x}^{(i)} \right\rangle \left\langle \mathbf{x}^{(i)} \middle| A^{(i)} \right\rangle$$
$$= \left(\det V^{(i)}\right)^3 \int \mathrm{d}\mathbf{k} \left\langle A^{(i)\prime} \middle| \mathbf{k} \right\rangle \left\langle \mathbf{k} \middle| \sqrt{\left(\vec{\pi}_{N-1}^{(i)}\right)^2 + m_i^2} \middle| \mathbf{k} \right\rangle \left\langle \mathbf{k} \middle| A^{(i)} \right\rangle. \quad (7.13)$$

The kernel of the integral in Eq. (7.13) can be evaluated as:

$$\left\langle \mathbf{k}' \middle| \sqrt{\left(\vec{\pi}_{N-1}^{(i)}\right)^2 + m_i^2} \middle| \mathbf{k} \right\rangle = \delta\left(\mathbf{k} - \mathbf{k}'\right) \sqrt{\hbar^2 \vec{k}_{N-1}^2 + m_i^2}. \quad (7.14)$$

Inserting this into Eq. (7.13) gives:

$$\left(\det V^{(i)}\right)^3 \int \mathrm{d}\mathbf{k} \left\langle A^{(i)\prime} \middle| \mathbf{k} \right\rangle \left\langle \mathbf{k} \middle| \sqrt{\left(\vec{\pi}_{N-1}^{(i)}\right)^2 + m_i^2} \middle| \mathbf{k} \right\rangle \left\langle \mathbf{k} \middle| A^{(i)} \right\rangle$$
$$= \left(\det V^{(i)}\right)^3 \int \mathrm{d}\mathbf{k}\mathrm{d}\mathbf{q} \sqrt{\hbar^2 \mathbf{q}^2 + m_i^2} \left\langle A^{(i)\prime} \middle| \mathbf{k} \right\rangle \delta\left(\mathbf{k}_{N-1} - \mathbf{q}\right) \left\langle \mathbf{k} \middle| A^{(i)} \right\rangle. \quad (7.15)$$

The element $\langle \mathbf{x} | \mathbf{k} \rangle$ between the position and momentum is:

$$\langle \mathbf{x} | \mathbf{k} \rangle = (2\pi)^{-\frac{3}{2}(N-1)} \exp\left(i \mathbf{k}^{\mathrm{T}} \mathbf{x}\right). \quad (7.16)$$

This means that the product $\langle \mathbf{k}|A\rangle$ in Eq. (7.15) is a Gaussian [2]:

$$\begin{aligned}\langle \mathbf{k}|A\rangle &= \int \mathrm{d}^{3N}\mathbf{x}\,\langle \mathbf{k}|\mathbf{x}\rangle\,\langle \mathbf{x}|A\rangle \\ &= \int \mathrm{d}^{3N}\mathbf{x}\,(2\pi)^{-\frac{3}{2}(N-1)}\exp\left(i\mathbf{k}^{\mathrm{T}}\mathbf{x}-\mathbf{x}^{\mathrm{T}}A\mathbf{x}\right) \\ &= \exp\left(-\frac{1}{4}\mathbf{k}^{\mathrm{T}}A^{-1}\mathbf{k}\right)(\det A)^{-\frac{3}{2}}. \end{aligned} \tag{7.17}$$

To evaluate the inner product of the delta function in Eq. (7.15) it can be noted [13]:

$$\begin{aligned}&\int \mathrm{d}\mathbf{x}\,\left\langle A'\middle|\mathbf{x}\right\rangle\delta\left(\mathbf{x}_j-\mathbf{r}\right)\langle \mathbf{x}|A\rangle \\ &= \left(4\pi\left(A+A'\right)_{j,j}\right)^{-\frac{3}{2}}\exp\left(-\frac{1}{4}\left(A+A'\right)^{-1}_{j,j}\mathbf{r}\right)\left\langle A'\middle|A\right\rangle \\ &\qquad \text{for}\quad j=1,2,\ldots,N-1. \end{aligned} \tag{7.18}$$

The integral in Eq. (7.15) can be evaluated by applying the Eqs. (7.17) and (7.18):

$$\begin{aligned}&\left\langle A'\middle|\sqrt{\left(\vec{\pi}^{(i)}_{N-1}\right)^2+m_i^2}\middle|A\right\rangle \\ &= \left(\det V^{(i)}\right)^3\left(\det A^{(i)}\det A'^{(I)}\right)^{-\frac{3}{2}}\int \mathrm{d}\mathbf{k}\,\exp\left(-\frac{1}{4}\mathbf{k}^{\mathrm{T}}\left((A^{(i)})^{-1}+(A'^{(i)})^{-1}\right)\mathbf{k}\right) \\ &\quad\times\left(\frac{c_i}{\pi}\right)^{\frac{3}{2}}\int \mathrm{d}\mathbf{q}\mathrm{e}^{-c_i\mathbf{q}^2}\sqrt{\hbar^2\mathbf{q}^2+m_i^2} \\ &\quad= \left\langle A'\middle|A\right\rangle f(c_i,m_i), \end{aligned} \tag{7.19}$$

with

$$c_1^{-1} = \left(\left(V^{(i)}\right)^{\mathrm{T}}A(A+A')^{-1}A'V^{(i)}\right)_{N-1,N-1}, \tag{7.20}$$

and the function f defined by:

$$f(x,m) = \left(\frac{x}{\pi}\right)^{\frac{3}{2}} \int \mathrm{d}\mathbf{q}\, \mathrm{e}^{-x\mathbf{q}^2} \sqrt{\hbar^2\mathbf{q}^2 + m^2}$$
$$= 4\pi \left(\frac{x}{\pi}\right)^{\frac{3}{2}} \int_0^\infty \mathrm{dq}\, \mathrm{e}^{-xq^2} \sqrt{\hbar^2 q^2 + m^2} q^2. \tag{7.21}$$

The function f in Eq. (7.21) is not analytic, but can be solved using numeric analysis [4] .

By inserting the result in Eq. (7.19) back into Eq. (7.2) from the start of this section the matrix relativistic kinetic energy can be calculated. Due to the non analytic nature of the solution the relativistic calculation requires a significant larger computational load than the classical counterpart.

8

Numerical method

Before discussing the calculated results in section Chapter 9 and Sections 10.1 to 10.3, some general aspects of the numerical analysis are discussed in this section.

In this thesis the neutron and proton are set to have the same mass to simplify the calculations. The mass of the nucleons is $m_n = m_p = 929\,\text{MeV}$ and the reduced Planck constant times the speed of light is $\hbar c = 197.327\,\text{Mev fm}$ [9].

8.1 Generation of Gaussians

In the correlated Gaussian method described in Chapter 6 the Gaussians are generated from stochastic variables. Eq. (6.2) describes how the matrices in Eq. (6.1) are constructed from a number of stochastic range parameters $b_{i,j}$. The range parameter must be taken from an appropriate distribution, in this thesis the distribution is given by:

$$b_{i,j} = -\ln(u)b, \tag{8.1}$$

where b is the scale and $u \in]0,1[$ is a stochastic variable. In this thesis the stochastic variable is taken from a Van der Corput sequence. The scale b is set to 6 fm when generating two-body Gaussians, 7 fm when generating three-body Gaussians and 8 fm when generating four-body Gaussians.

Using a quasi-random Van der Corput sequence as opposed to a pseudo-random sequence offers a number of advantages. Firstly, given consistent input parameters, the Van der Corput sequence always produces

the same output. Hence, the Gaussians remain constant over repeated numerical simulations. This makes the process of reproducing results simple and makes optimization of the model parameters consistent. Secondly, the quasi-random sequences have low-discrepancy [3]. The low-discrepancy is expected to result in a better description of the physical system compared to the high discrepancy pseudo-random sequence [3]. This also results in a lower number of required Gaussians to simulate the system, hence decreases the computational load of the calculations. The low-discrepancy sequence minimizes the overlap between the Gaussians. This is desired since large overlap between states can result in computational errors.

8.2 Solving the generalized eigenvalue problem

Solving the generalized eigenvalue problem Eq. (5.2) demands some considerations. Since the overlap matrix $\mathcal{N}$ is hermitian and positive-defined, the matrix can be decomposed into the product of a lower triangle matrix and its transposed by using Cholesky decomposition [4]:

$$\mathcal{N} = LL^{\mathrm{T}}, \tag{8.2}$$

where L is a lower triangle matrix and its transposed is an upper triangle matrix. This allows the generalized eigenvalue problem of Eq. (5.2) to be written on the form:

$$L^{-1}\mathcal{H}L^{-\mathrm{T}}L^{\mathrm{T}}c = \mathcal{H}'c' = E'c', \tag{8.3}$$

where $\mathcal{H}' = L^{-1}\mathcal{H}L^{-\mathrm{T}}$ is a matrix with same dimensionality as $\mathcal{H}$ and $c' = L^{\mathrm{T}}$ is a column vector with same number of elements as c. In Eq. (8.3) the generalized eigenvalue problem has the form of a classic eigenvalue problem, which can be solved using the Jacobi eigenvalue algorithm [4].

Both Cholesky decomposition and the Jacobi eigenvalue algorithm have complexity of $O(n^3)$ [4]. The $\mathcal{H}'$ matrix has dimensions equal to the number of all Gaussians (regardless of Gaussians dimensionality) used in the simulation. Consequently the computational load increases significantly for large numbers of Gaussians. To minimize the computational load it is therefore desirable to find the smallest number of Gaussians required to simulate the system in a satisfying level of detail.

If two or more Gaussians have a large overlap, the process of solving the generalized eigenvalue problem can become numerical unstable, hence the code becomes unable to compile.

8.3 Optimizing the model parameters

Given that the Gaussians offer a satisfying description of the system, the free parameters of the model will be chosen so that the results correspond to experimental findings. The model parameters in question are the mass of the sigma-meson m_σ and the two parameters in the coupling operator, see Eqs. (4.14) and (4.16). In this simulation the mass of the sigma-meson is set to a reasonable value between 100 MeV and 1000 MeV. Then the two remaining model parameters are tuned until the simulation matches the experimental values for the ground state energy and charge radius.

The experimental values for the ground state energy and charge radius for the deuteron used in this thesis are $E^{(exp)} = -2.22\,\text{MeV}$, and $R_{c,}^{(exp)} = 2.13\,\text{fm}$ [9]. A measurement for the difference between the calculated results and the expectation is given by the root square sum of relative errors:

$$V = \sqrt{\left(\frac{E^{(mod)} - E^{(exp)}}{E^{(exp)}}\right)^2 + \left(\frac{R_c^{(mod)} - R_c^{(exp)}}{R_c^{(exp)}}\right)^2}, \tag{8.4}$$

where $E^{(mod)}$ and $R_c^{(mod)}$ are the computed values for the ground state energy and charge radius respectively.

Eq. (8.4) is minimized by applying the downhill simplex method, to tune the model parameters [4] [10]. For each iteration of the downhill simplex the generalized eigenvalue problem is solved, hence requiring a high computational load.

8.4 Numerical integration

Calculating the matrix elements for the relativistic kinetic energy requires evaluating the non-analytic f function in Eq. (7.21). This numerical integration is computed using an adaptive quadrature [4]. By requiring numerical integration the calculation of the matrix elements for the relativis-

tic kinetic energy has a substantially larger computational load compared to calculating the classical alternative.

9

Results I: Verification of previous results

The examinations of the the explicit meson model in [1] and [6] have applied different coupling terms resulting in different levels of success.

In this section the results in [1] and [6] will be recreated. Firstly, in Section 9.1 the explicit meson model will be used to simulate the deuteron system using the coupling operator in Eq. (4.16) to verify the results in [1]. Secondly, in Section 9.2 the simulation is attempted using the coupling operator in Eq. (4.14) to verify the results in [6]. Note that all simulations in this section use the one-meson approximation, as it is the case in [1] and [6].

9.1 Deuteron with D. V. Fedorov's coupling

The study performed by D. V. Fedorov in [1], where a deuteron system was simulated in the explicit meson model with the coupling term given in Eq. (4.14), produced a satisfying simulation of the system. In this subsection these results will be recreated.

In Chapter 8 it is described how the free parameters in the coupling term are tuned for any given meson mass. It turns out that for a sufficiently large number of Gaussians the root square sum of relative error becomes acceptable. Concretely given $n_{(2)} = 20$ two-body Gaussians and $n_{(3)} = 100$ three-body Gaussians, then for any given mass of the sigma-meson in the interval between 10 MeV and 1000 MeV, the two free model

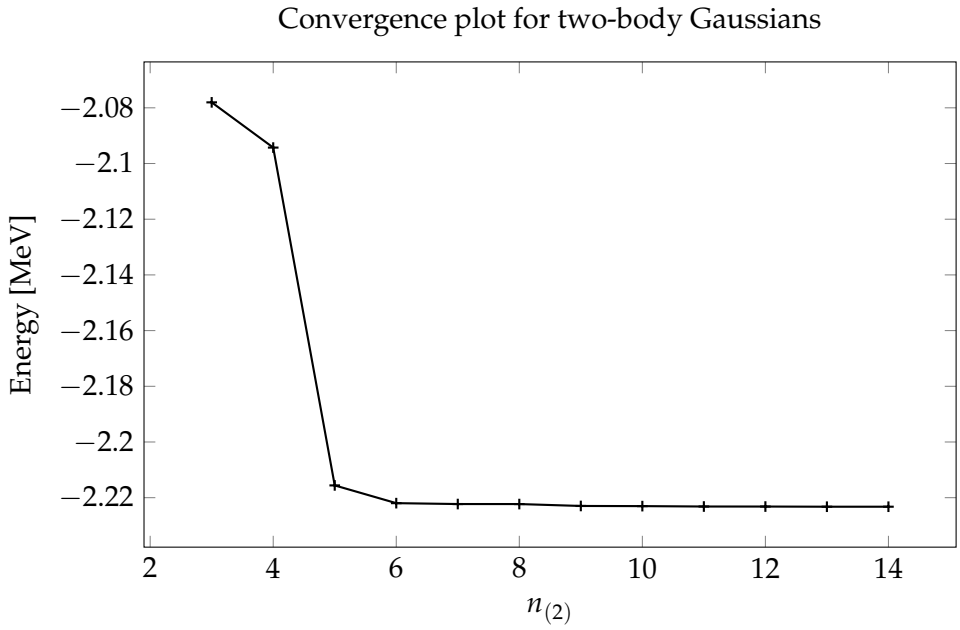

Figure 9.1: The deuteron ground-state energy E_0 calculated with $n_{(2)}$ two-body Gaussians and 100 three-body Gaussians. The applied coupling operator is seen in Eq. (4.16).

parameters can be chosen so that the root square sum of relative error becomes below 0.01.

An example: If the number of Gaussians is $n_{(2)} = 20$ two-body Gaussians and $n_{(3)} = 100$ three-body Gaussians with a mass of the sigma-meson set to $m_\sigma = 500\,\text{MeV}$, then the root square sum of relative errors becomes $V = 8.4 \cdot 10^{-4}$. The free model parameters are found to $S_\sigma = 18.39\,\text{MeV}$ and $b_\sigma = 3.134\,\text{MeV}$, which result in a ground state energy $E_0 = -2.223\,\text{MeV}$ and a charge radius of $R_c = 2.129\,\text{fm}$ for the deuteron system.

Figs. 9.1 and 9.2 show the convergence of ground state energy for a varied number of Gaussians. In Fig. 9.1 the number of two-body Gaussians is varied and in Fig. 9.2 the number of three-body Gaussians is varied. Both figures show that the ground state energy converges within a reasonable number of Gaussians. This allows the deuteron system to be analyzed using a relative low computational capacity. When the number of three-body Gaussians is set to 100, the ground state energy converges

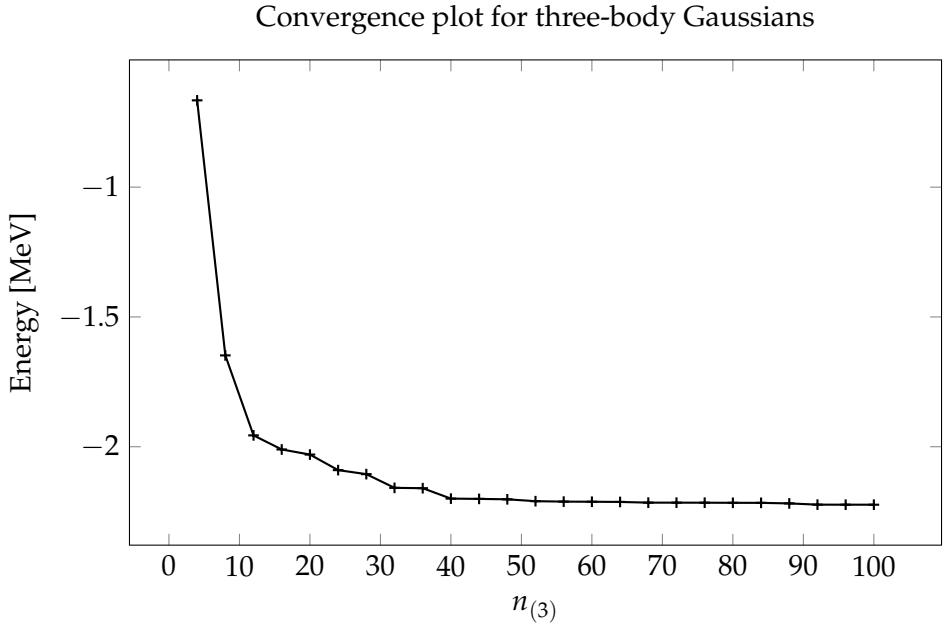

Figure 9.2: The deuteron ground-state energy E_0 calculated with $n_{(3)}$ three-body Gaussians and 20 two-body Gaussians. The applied coupling operator is seen in Eq. (4.16).

within 1 % with 5 two-body Gaussians. If the number of two-body Gaussians is set to 20, the ground state energy converges within 1 % with 50 three-body Gaussians.

For the two-body neutron-proton deuteron subsystem the wave-function can be computed, see Eqs. (6.1) and (6.6). The radial wave-function is given as $u(r) = r\psi_{(2)}(r)$, where $\psi_{(2)}$ is the wave-function of the two-body deuteron subsystem. Fig. 9.3 illustrates the radial wave-function with the asymptotic form $\exp(-\kappa r)$, where $\kappa = \sqrt{\frac{2\mu_{(2)}|E_0|}{\hbar^2}}$ and $\mu_{(2)}$ is the reduced mass of the subsystem. The radial wave-function follows the asymptotic curve. This is the asymptotic behavior associated with the deuteron [14].

The results in this section confirm the results presented by D. V. Fedorov in [1]. The differences between the exact numerical values in this subsection and [1], are the result of the two simulations using different Gaussians throughout the calculations.

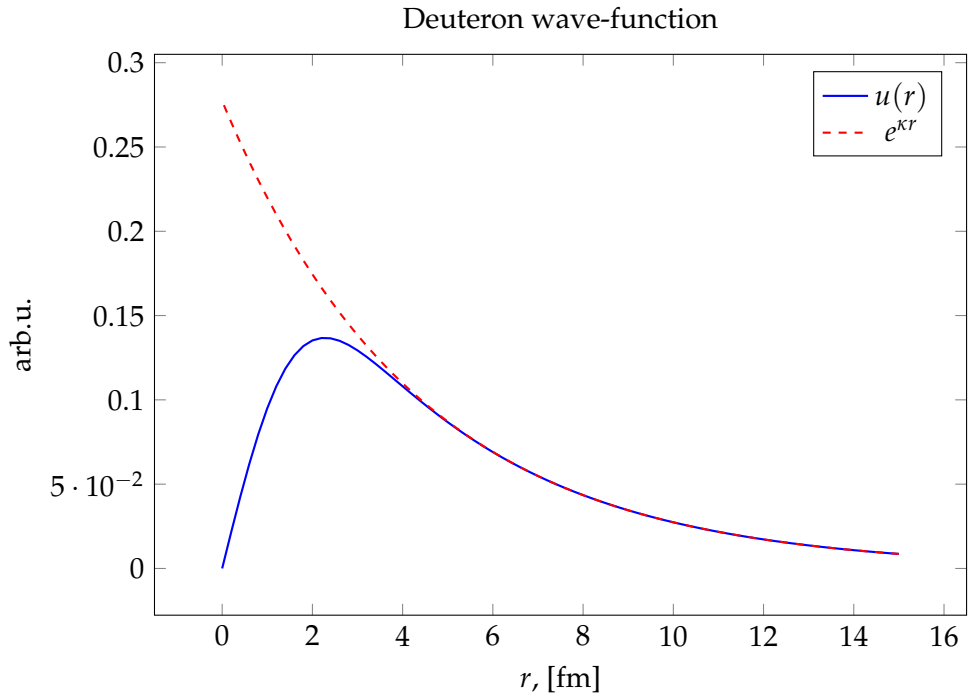

Figure 9.3: The radial wave-function for the neutron-proton subsystem of deuteron and the asymptotic form, $\exp(-\kappa r)$. The applied coupling operator is seen in Eq. (4.16).

9.2 Deuteron with Filip Jensen's coupling

In this subsection a deuteron system will be simulated applying the explicit meson model using the coupling term proposed by Filip Jensen, given in Eq. (4.14) [6]. The coupling allows the nucleons to emit mesons even outside the proximity of other nucleons. This makes the coupling operator more realistic than Eq. (4.14) used in 9.1. Previous simulations of the explicit meson model using this coupling have been performed by Filip Jensen [6]. These simulations found that the model was unable to produce results matching experimental findings [6]. This is in contrast to the simulation performed by D. V. Fedorov [1].

In Fig. 9.4 the convergence of the ground state energy is shown as the number of Gaussians in the two-body subsystem increases, the number of Gaussians in the three-body subsystem remains constant at $n_{(\sigma)} = 100$.

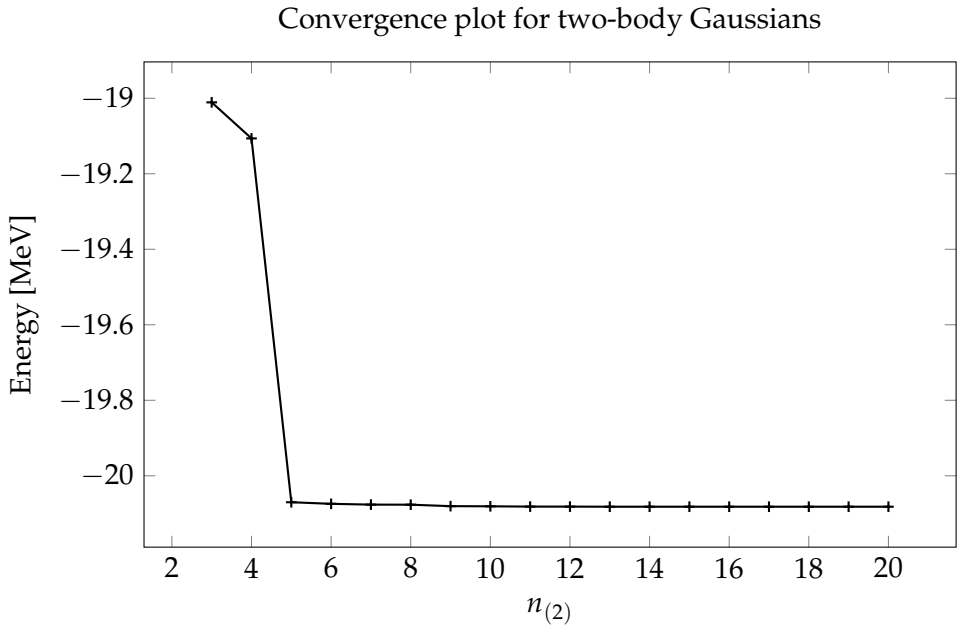

Figure 9.4: The deuteron ground-state energy E_0 calculated with $n_{(2)}$ two-body Gaussians and 100 three-body Gaussians. The applied coupling operator is seen in Eq. (4.14).

The ground state energy converges within 1 % with about 6 Gaussians. Fig. 9.5 shows the ground state energy convergence, if the number of Gaussians in the two-body subsystem is held constant at 20 and the number of three-body Gaussians is varied. Here the ground state energy converges far slower compared to Fig. 9.2. To achieve a convergence of the ground state energy within 1 % about 360 Gaussians are required. Note that the larger number of required three-body Guassians increases the computational load significantly compared to Section 9.1.

With a mass of the sigma-meson set to $m_\sigma = 500\,\text{MeV}$ the free parameters in the model could not be tuned in a way such that the root square sum of relative errors has a value lower than $V = 1.6$. This is despite using a large number of Gaussians in the three-body subsystem. The best result, using 20 Gaussians in the two-body subsystem and 300 Gaussians in the three-body subsystem, gave the root square sum of relative errors of $V = 1.688$. Here the calculated ground state energy becomes $E_0 = -4.079\,\text{MeV}$ and the calculated charge radius becomes

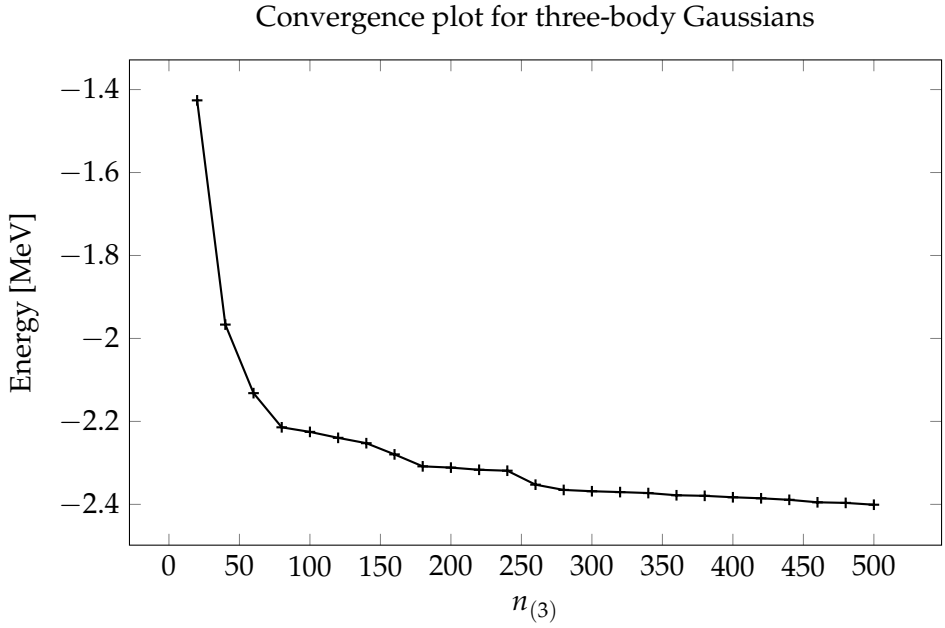

Figure 9.5: The deuteron ground-state energy E_0 calculated with $n_{(3)}$ three-body Gaussians and 20 two-body Gaussians. The applied coupling operator is seen in Eq. (4.14).

$R_c = 5.253\,\text{fm}$. The strength parameter was tuned to $g = 14.19\,\text{MeV}$ and the range parameter was tuned to $\gamma = 6.908\,\text{fm}$.

The large differences between the computed values and the experimental findings imply that the explicit meson model with the coupling in Eq. (4.14) is unable to simulate a deuteron system. A possible solution to this problem is to incorporate the "dressing" of nucleons by mesons into the model. This will be examined in the two following sections Sections 10.1 and 10.2.

10

Results II

In this chapter the results not previously published are presented.

10.1 Filip Jensen's coupling with dressed nucleons

In Section 9.2 it was shown that the explicit meson model in the one-meson approximation with the coupling operator that is given in Eq. (4.14), is unable to describe a deuteron system. The model is unable to produce a ground state energy and a charge radius that correspond to the experimental data.

In this section additional complexity will be introduced into the model, by including the correction from bound nucleon-meson states, the so called "dressing" of nucleons.

The coupling operator in Eq. (4.14) allows a nucleon to emit mesons regardless of whether the nucleon is in the proximity of any other nucleons or not. This opens the possibility for bound nucleon-meson states. In the one-meson approximation a nucleon-meson system will become a superposition of a one-body nucleon subsystem and a two-body nucleon-meson subsystem. Performing a coordinate transformation, see Chapter 3, and subtracting the center-of-mass coordinate reduces the system to a single coordinate. Hence, analyzing the system only requires Gaussians in the two-body subsystem. It is natural to reuse the Gaussians in the deuteron two-body subsystem.

The correction from the nucleon-meson states can be included into the model by calculating the ground state energies for the nucleon-meson

subsystem. Then subtracting the ground state energies of the two nucleons from the deuteron energies.

It should be noted that zero energy is set equal to the total mass of the nucleons, hence the correction from the dressing of the nucleons must be subtracted from the result.

The inclusion of the correction from the nucleon-meson states, requires a larger computational load when simulating the system. This added complexity originates from the solution of the generalized eigenvalue problem for the nucleon-meson subsystem. It should be noted that the simulation of the nucleon-meson system only requires a small fraction of the computational load required to simulate the full deuteron system. The nucleon-meson system uses the same coupling term as the deuteron system. Therefore the two free parameters in the coupling can only be tuned to the experimental data after the correction from the nucleon-meson states is included into the model. The tuning of the free model parameters is described in more detail in Chapter 8.

By including the correction from the bound nucleon-meson states, the free-parameters can be tuned so that the root square sum relative errors, see Eq. (8.4), become lower than 0.01 for any mass of the sigma-meson between 10 MeV and 1000 MeV. This is similar to the result in Section 9.1, where the coupling operator applied is Eq. (4.15). The result is implying that including the correction from the bound nucleon-meson states is necessary when using the Filip Jensen's coupling operator, in Eq. (4.14).

If the mass of the sigma-meson is set to $m_\sigma = 500\,\text{MeV}$ the free-parameters can be tuned so that the strength becomes $g = 77.49\,\text{MeV}$ and the range becomes $\gamma = 2.088\,\text{fm}$. This gives a ground state energy of $E_0 = 2.230\,\text{MeV}$ and a charge radius of $R_c = 2.127\,\text{fm}$, corresponding to a root square sum of relative errors of $V = 0.0021$. The ground state energy of the nucleon-meson becomes $-14.20\,\text{MeV}$. Compared to the result for the same meson mass in Section 9.1 the strength and range parameters differ.

The figures Figs. 10.1 and 10.2 show the convergence of the ground state energy for varying numbers of Gaussians. Fig. 10.1 shows the convergence of the energy for varying numbers of two-body Gaussians, when the number of three-body Gaussians is constant. At first glance the convergence of the energy in Fig. 10.1 looks nonphysical, since the expectation from the variation principle is that the energy falls as the description of the system increases. The reason for the increasing energy is that

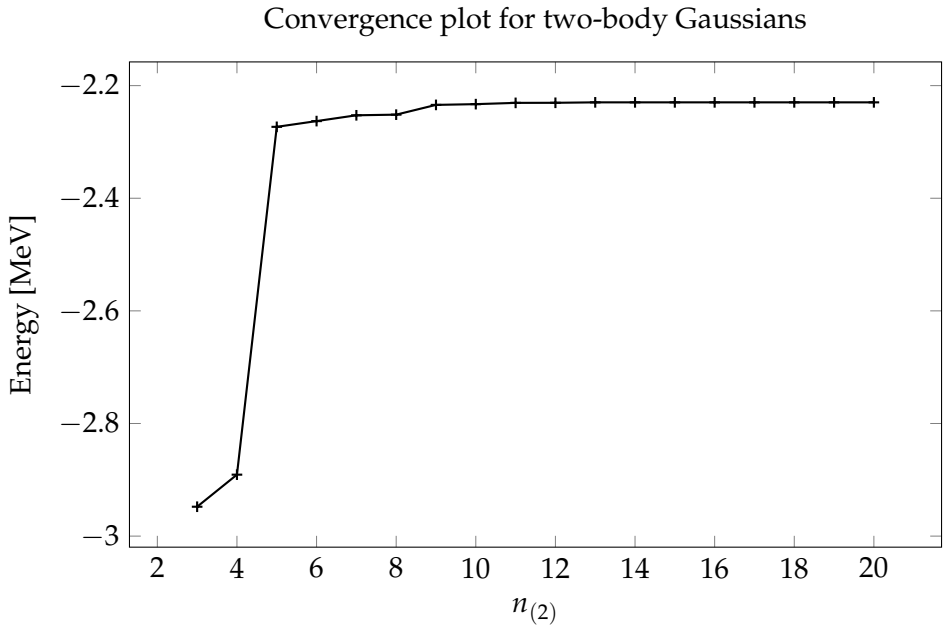

Figure 10.1: The deuteron ground state energy E_0 calculated with $n_{(2)}$ two-body Gaussians and 100 three-body Gaussians. The applied coupling operator is given in Eq. (4.14). The calculation includes the correction from dressed nucleon states.

the ground state energy of the two nucleon-meson systems is subtracted from the deuteron ground state energy. Since the energy of the nucleon-meson system converges slower than the energy of the deuteron system, the convergence curve increases. The energy converges within 1 % with about 9 Gaussians in the two-body subsystem. This is slower than the convergence in Section 9.2.

In Fig. 10.2 is shown the convergence of the ground state energy when the number of Gaussians in the three-body subsystem is varied and the number of Gaussians in the two-body subsystem constant. The convergence curve has the expected form, since the energies of the nucleon-meson systems are independent of the three-body Gaussians. The ground state energy converges within 1 % in about 76 Gaussians. This is substantially faster than in Fig. 9.5 in Section 9.2.

The radial wave-function can be computed for the neutron-proton subsystem by the method described in Section 9.1. In Fig. 10.3 the re-

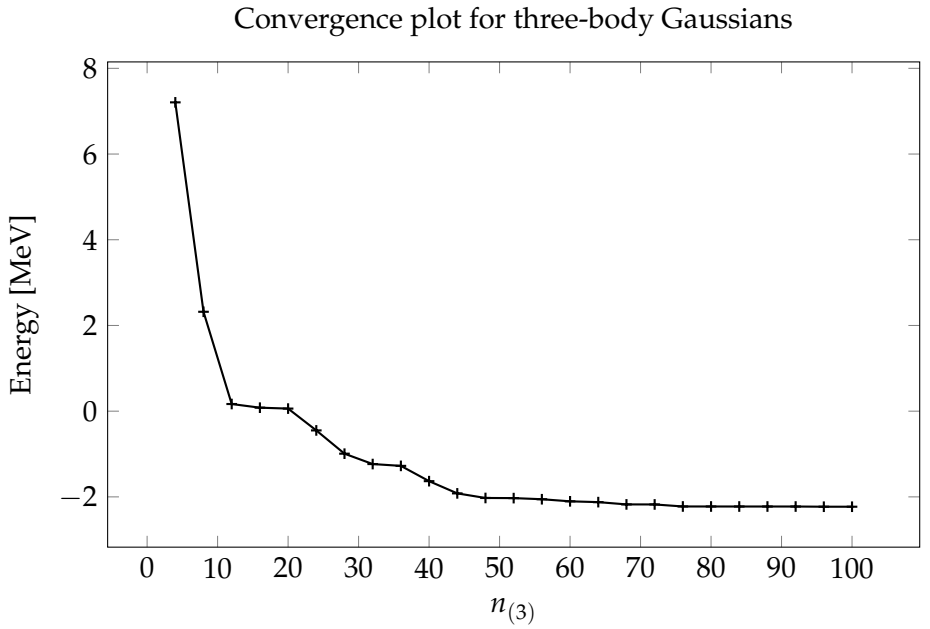

Figure 10.2: The deuteron ground state energy E_0 calculated with $n_{(3)}$ three-body Gaussians and 20 two-body Gaussians. The applied coupling operator is given in Eq. (4.14). The calculation includes the correction from dressed nucleon states.

sulting curve is shown together with the wave-function from Fig. 9.3. The comparison of the two curves illustrates that the wave-function calculated in this section is slightly different compared to the previous result. The asymptotic behavior of the wave-function calculated with Filip Jensen's coupling does not match the exponential $\exp(-\kappa r)$ where $\kappa = \sqrt{\frac{2\mu_{(2)}|E_0|}{\hbar^2}}$. An explanation for the asymptotic behavior of the wave-function, which does not match the expectations, is that the model only incorporates the one-meson approximation. In Section 10.2 the contribution from a second meson will be examined.

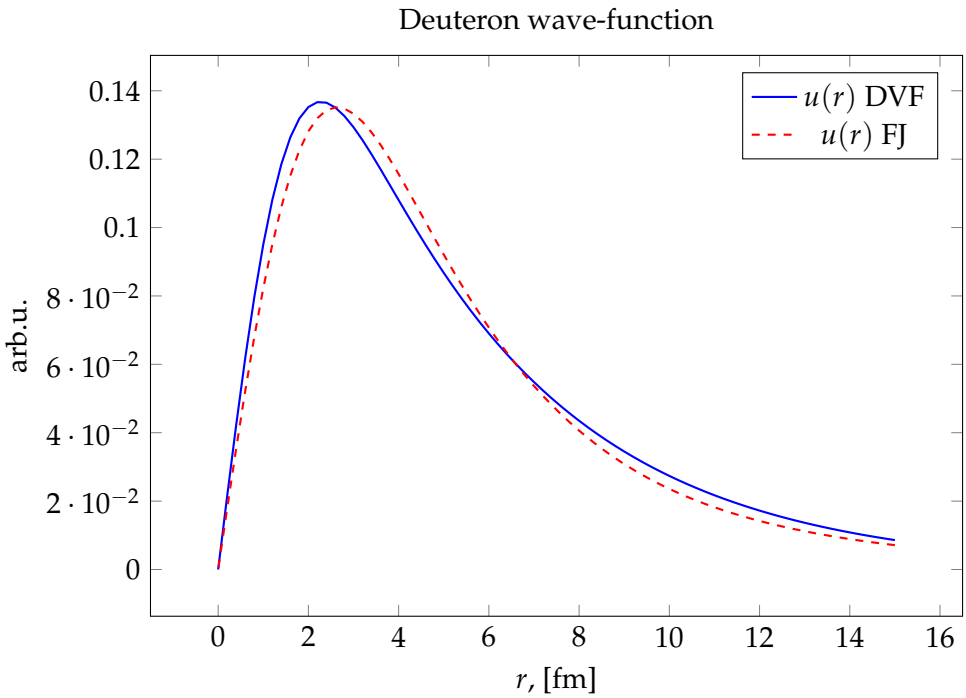

Figure 10.3: The radial wave-function for the neutron-proton subsystem of deuteron for the coupling term given in Eq. (4.16), denoted "DVF" and the coupling term given in Eq. (4.14), denoted "FJ". Both wave-functions computed in the one-meson approximation, with the inclusion of correction from bound nucleon-meson states.

10.2 Contribution from higher order approximations

In Section 10.1 the correction from dressed nucleon states is included into the deuteron model with the coupling term Eq. (4.14) in the one-meson approximation. This model is able to describe a deuteron system with ground state energy and charge radius corresponding to the experimental findings. In Section 10.1 the model was limited to the one-meson approximation, hence the contribution from higher order mesons is unexplored. In this section the contribution from a higher number of meson is investigated. Firstly by comparing the ground state energies of the nucleon-meson system and its higher order counterparts. Secondly by investigating the radial wave-function in the two-meson approximation to expand the result in Fig. 10.3.

10.2.1 Comparing the ground state energies of the nucleon system in higher order approximations

When the ground state energy of systems consisting of a varying number of mesons and a single nucleon is compared, a approximation of the contribution from higher meson numbers to the full deuteron system is obtained. To ensure comparable results the free parameters in the coupling term are constant throughout the calculations. The free parameters applied in this section are the same ones that were calculated in Section 10.1.

In the explicit meson model the nucleon-meson-meson system becomes a superposition of a one-body nucleon subsystem, a two-body nucleon-meson subsystem and a three-body nucleon-meson-meson subsystem. Hence, the Hamiltonian $\mathcal{H}$ in the generalized eigenvalue problem has dimensionality $n_{(2)} + n_{(3)} + 1$, where $n_{(2)}$ and $n_{(3)}$ are the numbers of Gaussians in the two-body and three-body subsystems respectively. It follows that a nucleon-meson-meson-meson system becomes a superposition of four subsystems.

Fig. 10.4 shows ground state energies of a nucleon-meson system, a nucleon-meson-meson system and a nucleon-meson-meson-meson system. The absolute value of ground state energy increases with higher numbers of mesons for all meson masses. The difference between the system with two and three mesons respectively is relatively small, making differentiating between the curves difficult. A local minimum for the

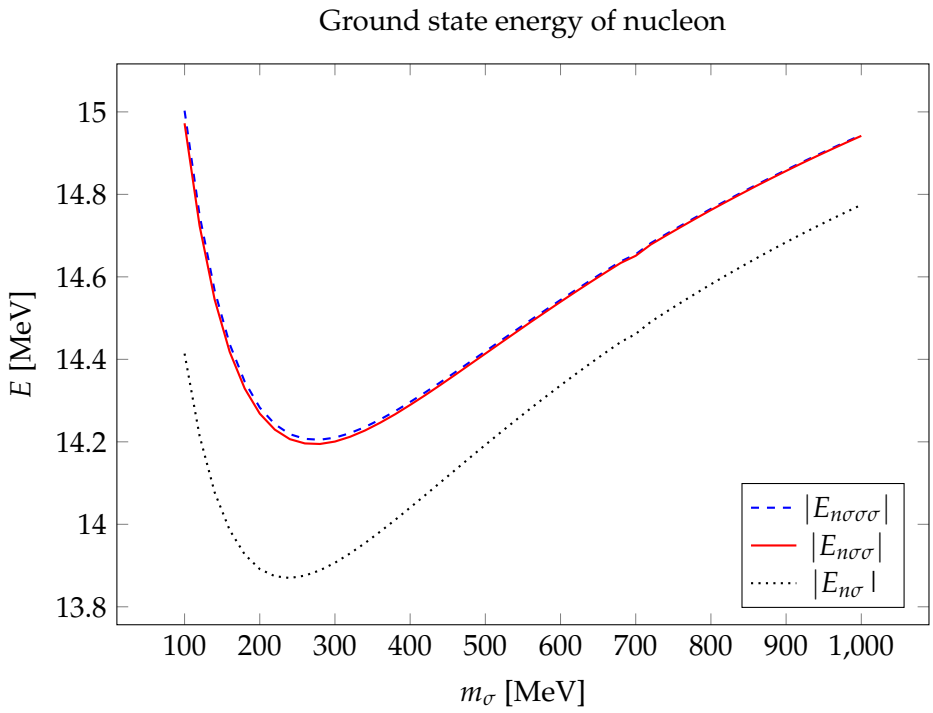

Figure 10.4: Ground state energy for a nucleon-meson system, $E_{n\sigma}$, a nucleon-meson-meson system, $E_{n\sigma\sigma}$, and the nucleon-meson-meson-meson system,$E_{n\sigma\sigma\sigma}$. The energies are calculated using the interaction in Eq. (4.14) and mass m_σ. The free parameters in the coupling term Eq. (4.14) are tuned so the ground state energy and charge radius of the deuteron in the one-meson approximation match the experimental findings.

ground state energies is found for a meson mass between 200 MeV and 300 MeV. The reason for the appearance of a local minimum is found in the coupling term. Since the free parameters are refitted for every given meson mass, the coupling is not consistent between different meson masses. If the coupling operator was held constant, the ground state energies will decrease as the mass increases, see Fig. B.1.

In the explicit meson model the cost of meson emission is dependent of the meson mass, hence the contribution from higher order approximations decrease for high masses. This is illustrated in Fig. 10.5. The figure shows the relative difference between the ground state energy of the nucleon systems of differing meson numbers. Even for low meson masses

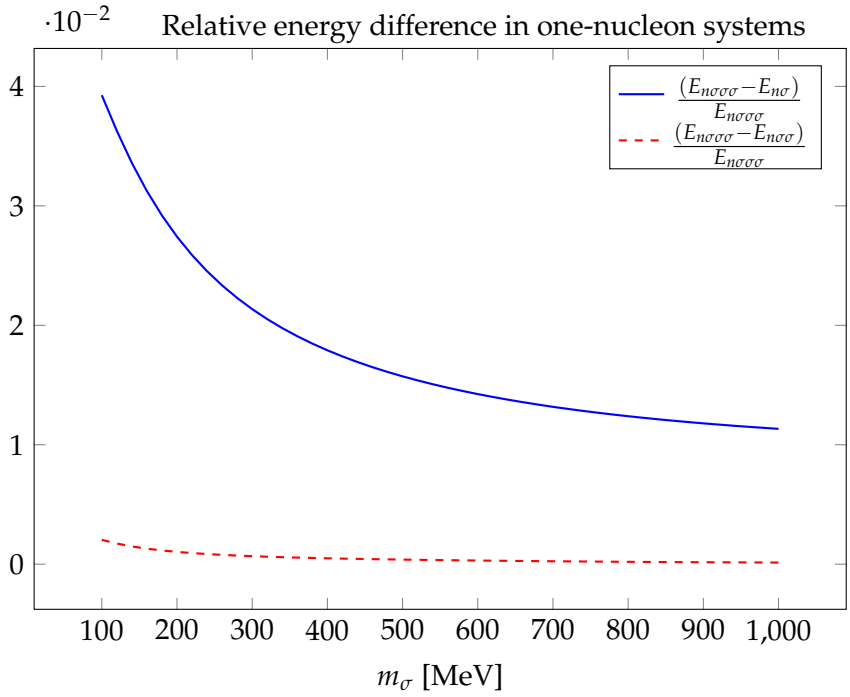

Figure 10.5: Relative difference in ground state energies between a nucleon-meson system, with energy $E_{n\sigma}$, and a nucleon-meson-meson-meson system, with energy $E_{n\sigma\sigma\sigma}$, and the relative difference between a nucleon-meson system, with energy $E_{n\sigma\sigma}$, and a nucleon-meson-meson-meson system. The energies is calculated using the interaction in Eq. (4.14). m_σ denote the meson mass. The free parameters in the coupling term Eq. (4.14) are tuned so the ground state energy and charge radius of the deuteron in the one-meson approximation match the experimental findings.

the relative energy difference is below 4 % for the nucleon-meson. Hence, if a further study of the explicit meson model is incorporating pions the higher order corrections is only relevant for high precision calculations. For a meson mass of $m_\sigma = 500\,\text{MeV}$ the relative error becomes under 2 % in the two meson system. The relative difference between the two and three meson system is below 0.3 %.

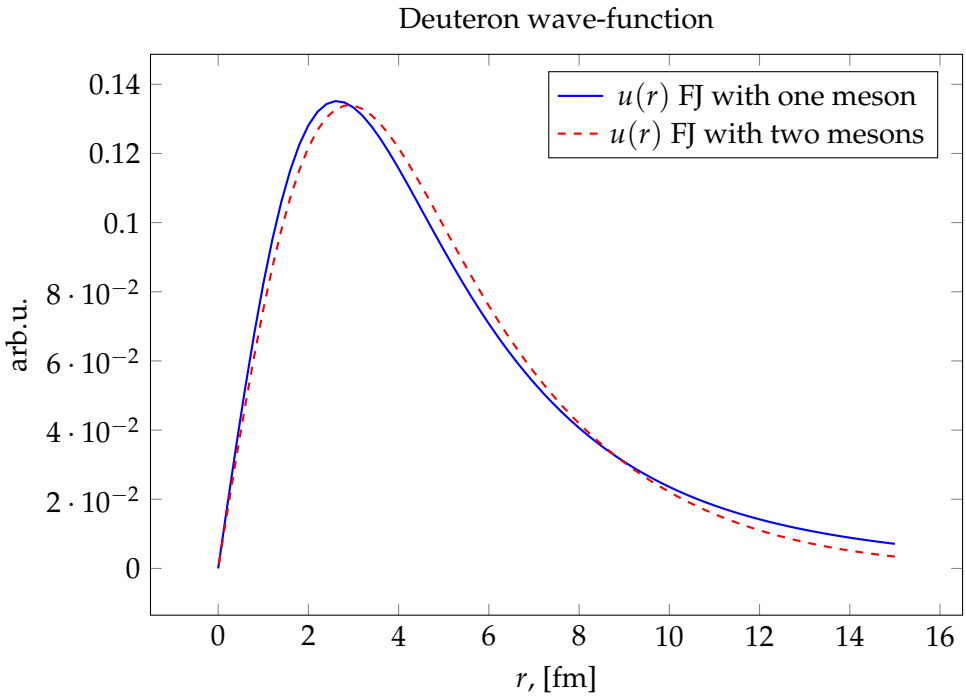

Figure 10.6: The radial wave-function for the neutron-proton subsystem of deuteron calculated in the one-meson and two-meson approximation respectively. The applied coupling operator is given in Eq. (4.14).

10.2.2 Radial wave-function for higher order approximations

In Section 10.1 the radial wave-function for the deuteron system in the one-meson approximation is examined. Fig. 10.3 depicts the found radial wave-function. The asymptotic behavior of the wave-function does not match the exponential $\exp(-\kappa r)$ with $\kappa = \sqrt{\frac{2\mu|E_0|}{\hbar^2}}$. To investigate the asymptotic wave-function for higher order approximations the wave-function is computed in the two-meson approximation, with the nucleon-meson-meson correction. Convergence plots for the deuteron in the two-meson approximation are seen in Figs. B.2 to B.4 in the appendix. Table B.1 features an example of the tuned model.

In Fig. 10.6 the radial wave-function for the deuteron system in the two-meson approximation is depicted with the radial wave-function in the one-meson approximation. The asymptotic form of radial wave-function

in the two-meson approximation does not match the exponential $\exp(-\kappa r)$. Hence, the result does not fully match the expectations and the behavior seen in [1].

10.3 Inclusion of relativistic kinetic energy

In Chapter 9 and Sections 10.1 and 10.2 a deuteron system was simulated in the explicit meson model using the classical (nonrelativistic) kinetic energy.

In this section it is examined if the non-relativistic approximation is reasonable. The first comparison between the classical and relativistic model is using the coupling operator proposed by D. V. Fedorov, in Eq. (4.15), since this coupling yields the simplest model. A description of the relativistic kinetic energy is given in Chapter 7.

The non-analytic matrix element for the relativistic kinetic energy in Eq. (7.19) depends on the meson mass. For high meson masses the relativistic kinetic energy is expected to approach the classical value.

To compare the relativistic and classical energies the coupling operator must remain fixed between the two models. Hence, the free-parameters in the operator must remain fixed. The tuning of the free model parameters by minimizing the sum of relative errors is described in Chapter 8. First the free-parameters are tuned using the non-relativistic kinetic energy for a given meson mass. Then the corresponding ground state energy and charge radius are calculated in the relativistic model.

It should be noted that the solution of the generalized eigenvalue problem is sensitive to even small numerical changes. For large matrices this problem can lead to significant errors. Hence, to avoid errors using a small number of Gaussians that still describes the system to a satisfying level of detail, is preferable.

In Fig. 10.7 the ground state energies for the classical and the relativistic models are shown. The free-parameters in the coupling have been tuned in the classical model. The difference between the two models decreases for high meson masses. The difference in charge radius between the two models has the same behavior as the ground state energy, see Fig. B.5. In the simulation the number of Gaussians in the two-body subsystem is 6 and in the three-body subsystem 50. Fig. 10.8 shows the root square sum of relative errors given in Eq. (8.4) for the relativistic model. For a meson with a mass roughly equal to that of the pion $m_\pi \approx 140\,\text{MeV}$, the root square sum of relative errors is 0.82. Similarly for a meson mass of $m_\sigma = 500\,\text{MeV}$ the root square sum of relative errors is roughly 0.18. This implies that if the explicit meson model has to incorporate pions, the model would need to incorporate the relativistic kinetic energy to get

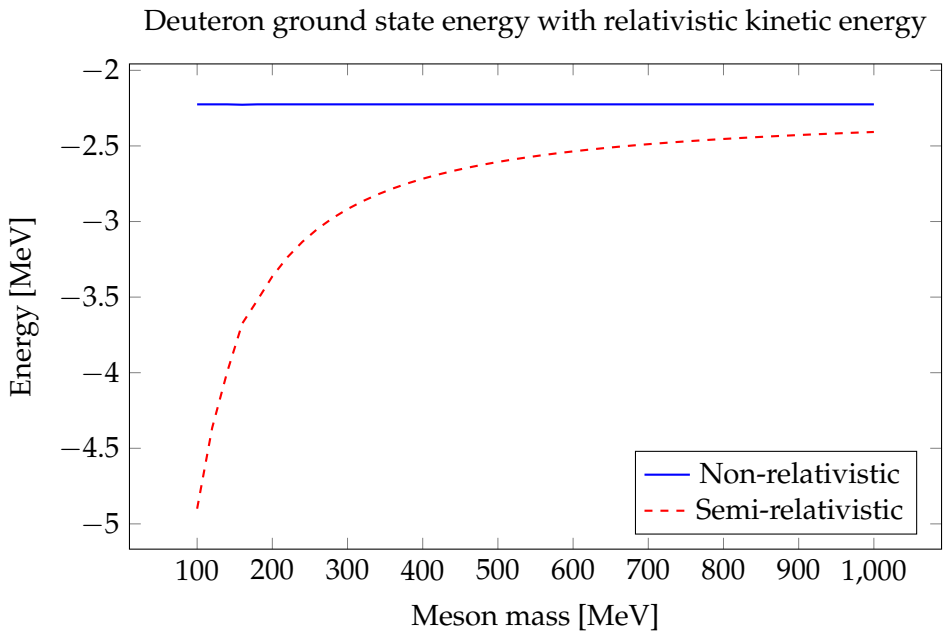

Figure 10.7: Ground state energy for the deuteron system calculated using the classical kinetic energy shown with the ground state energy calculated using the relativistic kinetic energy. The coupling operator applied in the model is Eq. (4.15). The free-parameters in the coupling operator, Eq. (4.15), are tuned so the calculated values of the ground state energy and the charge radius of deuteron with the classical kinetic energy match the experimental findings.

reliable results. In general the relativistic energy must be incorporated to achieve high precision results.

So far the free-parameters in the coupling term have been tuned in the classical model to estimate the difference between the classical and relativistic model. But if further studies are to be computed in a relativistic model, the tuning of the free-parameters must be archived in the relativistic model.

For any meson mass between 100 MeV and 1000 MeV the free-parameters in the coupling can be tuned so that the root square sum of relative errors becomes less than 0.01, in the relativistic model. Using the relativistic model with retuned free-parameters the results in previews chapters can be recreated. In the Appendix the results in Chapter 9 and Section 10.1 are recreated with relativistic kinetic energy, see Appendices B.4 to B.6.

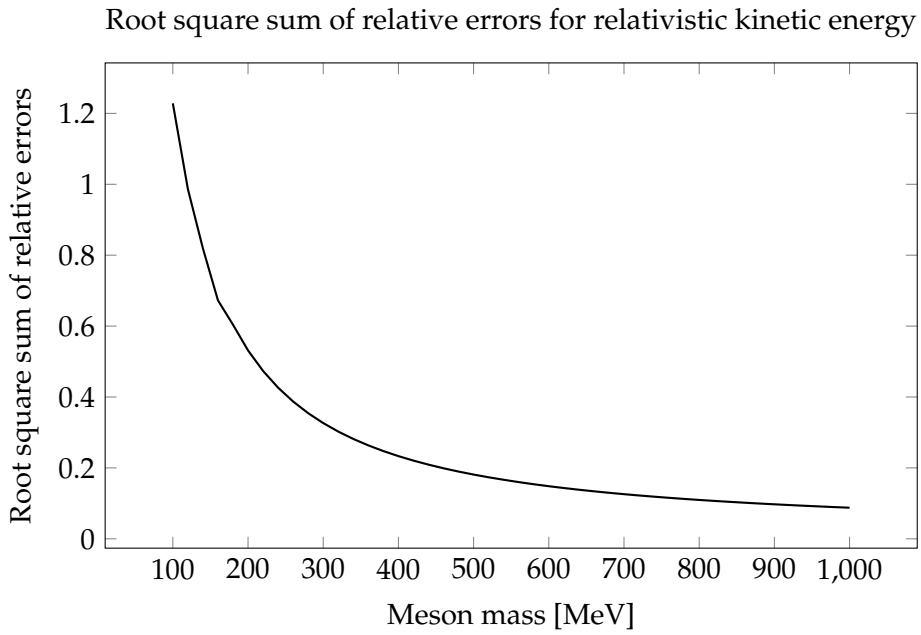

Figure 10.8: Root square sum of relative errors, see Eq. (8.4), for the ground state energy and charge radius calculated with relativistic kinetic energy. The free-parameters in the coupling operator, Eq. (4.15), is fitted with the classical kinetic energy to minimized the root square sum of relative errors, see Section 8.3.

11

Discussion

The explicit meson model has several potential advantages compared to established few-body nuclear models. One is that the explicit meson model has a lower number of model parameters. Another is that the explicit meson model includes few-body forces. The model also includes meson physics into the nucleon-nucleon interaction. In this thesis the only allowed meson is the sigma-meson.

Previously D. V. Fedorov has examined the explicit meson model in a deuteron system [1]. D. V. Fedorov used the coupling operator shown in Eq. (4.15) [1]. The coupling operator only allows meson production if both nucleons are in close proximity of each other [1]. D. V. Fedorov was able to fit the free-parameters in the model so the calculated ground state energy and charge radius matched the experimental expectations. The wave-function produced by the model has the asymptotic behavior that corresponds to the theoretical expectation. The calculated results in Section 9.1 confirm the previous findings. This implies that the model is successful in describing a deuteron system. The results in Section 9.1 and [1] have small numerical differences. This is most likely the result of the two simulations applying different Gaussians.

The explicit meson model has also been tested by Filip Jensen, who applied a more realistic coupling operator, seen in Eq. (4.14) [6]. The coupling allows for single nucleons to produce mesons independent of the position of other nucleons. Filip Jensen found that this coupling was unable to produce results that matched the experimental findings for the ground state energy and charge radius of deuteron. The "dressing" of nucleons from nucleon-meson states was not included in Jensens model.

In Section 9.2 Jensens simulation was recreated. The recreation confirmed that the experimental findings could not be obtained. This implies that the model in this form is unable to describe a deuteron system, without the inclusion of correction from the nucleon-meson systems introduced in Section 10.1. Other possible reasons for the unsuccessful results are that the number of applied Gaussians were unable to describe the system. It is also possible that the downhill simplex, see Section 8.3 used in the optimization of the free-parameters in the model got trapped in a local minimum.

The results in Section 9.2 and in [6], have some differences. A significant difference is that the number of applied Gaussians in [6] was significantly lower in both the two-body and three-body subsystems, compared to the results in Section 9.2. In Filip Jensen's calculations, [6], the ground state energy converges at a different rate than in Section 9.2. The difference is especially striking for the number of Guassians in the three-body subsystem, where the ground state energy seems to converge within 20 Gaussians in Filip Jensens' calculations as opposed to 360 Gaussians in Fig. 9.5. A likely explanation for the differences is that the Gaussians in the two analysis have been constructed differently, and the scale parameters were set to have different values. It is surprising that the ground state energy converges faster for Filip Jensen, since Jensen's Gaussians were constructed from a pseudo-random sequence where the Gaussians in this thesis are constructed using a quasi-random sequence, see Section 8.2. This is because the quasi-random sequence is expected to have faster convergence as compared to the pseudo-random sequence [3]. It is worth noting that the convergence plot in [6] is limited to 20 Gaussians in the three-body subsystem. Hence, it is possible that the ground state energy would have fallen further, if the number of Gaussians in the three-body subsystem had been allowed to surpass 20, offering a better description of the system.

The difference between the Gaussians in Section 9.2 and [6] is a probable reason for the difference in the root square sum of relative errors. In [6] the lowest value of the root square sum of relative errors was $V = 1.91(2)$ and in Section 9.2 the best result was $V \approx 1.6$. It is possible that this variation is due to the difference in the number and construction of the applied Gaussians. In [6] the number of applied Gaussians were 4 in the two-body subsystem and 11 in the three-body subsystem, where the numbers in Section 9.2 were 20 in the two-body subsystem and 300

in the three-body subsystem. In [6] the Gaussians have been taken from a pseudo-random sequence and optimized by replacing single Gaussians and recalculating the ground state energy, accepting the set of matrices that yields the lowest energy.

In Section 10.1 the correction from nucleon-meson state is included into the model applied in Section 9.2. For a given meson mass within a reasonable range the model achieves results close to the experimental findings. Compared with the result without the nucleon-meson correction, in Section 9.2, the ground state energy converges significantly faster for the number of Gaussians in the three-body subsystem. The convergence for Gaussians in the two-body subsystem was a bit slower, see Figs. 10.1 and 10.2. The reason that the ground state energy convergences at a slower rate for the Gaussians in the two-body subsystem, is likely due to the complexity added by the inclusion of the nucleon-meson states, since these systems also are described by the two-body Guassians. The three-body Gaussians converge faster, since some complexity from the nucleon-meson system has been removed. The total number of Gaussians was significant lower leading to a smaller computational load.

In Fig. 10.3 the radial wave-function is compared for the calculated models in Section 10.1 and Section 9.1. The wave-function calculated with Filip Jensen's coupling has a slightly different form compared to the wave-function calculated using D. V. Fedorov's coupling. This difference also gives the wave-function calculated with Jensen's coupling a different asymptotic behavior. The asymptotic form of the wave-function calculated with Jensen's coupling is different from the expected.

A possible explanation for why the wave-function computed with Filip Jensen's coupling does not appear to match expectations, is that the model is unable to describe the asymptotic behavior without the inclusion of higher meson numbers. In Fig. 10.6 the corresponding radial wave-function in the two-meson approximation is shown. The figure shows that the wave-function for the two-meson approximation is slightly different from one-meson approximation. The asymptotic behavior of the wave-function in the two-meson approximation does not match expectation. It is possible that still higher order approximations must be included to yield the expected form of the radial wave-function. Another possibility is that the model does not consider some interactions of the real system.

In Chapter 9 and Section 10.1 a deuteron system was simulated in the

one-meson approximation, where the nucleons is prohibited from producing more than one-meson. Due to meson states being under a potential barrier equal to the total mass of the emitted mesons, the contribution from higher meson numbers is expected to be small. The contribution from higher order approximations must be depending on the meson mass. In Section 10.2.1 the ground state energy of a system consisting of one nucleon with one to three mesons is calculated for varying meson masses. The energies are compared for different meson numbers in Figs. 10.4 and 10.5. For the approximate mass of pions, 140 MeV, the relative difference between the one-meson and three-meson systems is under 4 %, and the difference between the two-meson and three-meson systems is under 0.3 %. This result gives an estimate for the contribution from higher order approximations.

In [11] the dressing of protons by pions is investigated. In [11] Østerlund made an analysis of the contribution from the two-meson approximation to the pion dressing and how the strength and range parameters in the coupling term effect this contribution. These results are outside the scope of this thesis.

Due to the added complexity of the implementation and required computational load, future studies of the explicit meson model must evaluate the desired accuracy, and choose the practical number of allowed mesons. In systems of larger complexity it is possible that some properties of the system require a certain number of mesons to accurately simulate the systems.

In Section 10.3 the difference between the classical and the relativistic kinetic energy is investigated. Figs. 10.7 and 10.8 show that even for relative high meson masses the difference between the relativistic and classical energies is significant. Hence, the relativistic kinetic energy should, if possible, be used instead of the classical to achieve precise results. By refitting the free-parameters in the model the result in Chapter 9 and Sections 10.1 and 10.2 can be recreated using the relativistic kinetic energy. Since the matrix element for the relativistic kinetic energy is non-analytic, see Chapter 7, the calculations take a larger computational load compared to the classical energy.

The solution of the generalized eigenvalue problem is sensitive to even small changes in the matrix elements. But the fitting of the model parameters gives a small error in matrix elements of the coupling, and the numerical integration also leads to small errors in the matrix elements for

the kinetic energy. All the small errors can accumulate over large matrices leading to unreasonable results. To circumvent this problem a relative small number of Gaussians was applied to the system.

The classical kinetic energy is an approximation of the relativistic kinetic energy in the low velocity limit. Since the two energies give such different results when applied in the explicit meson model, it is worth considering why the classical kinetic energy still yields the results in Sections 9.1, 10.1 and 10.2 that imply that the model works as intended. The likely explanation for the results in Sections 9.1, 10.1 and 10.2 is that two free-parameters are fitted to two experimental values. Fitting two free parameters to two data points is expected to be achievable for any somewhat reasonable model. Hence, the model can produce results that match the experimental expectations even if there is a error in the calculation of some of the matrix elements.

In [8] Mikkelsen investigated the relativistic correction for a proton dressed with pions in the one-pion approximation. It was found that the relativistic correction was small for most values of the coupling operator. This is in contrast to the results found in Section 10.2. The dressed proton analyzed in [8] is a different system than the deuteron analyzed in this thesis, hence the results are not directly comparable. But given the analysis in [8] are correct, the result in [8] can still indicate an error in Section 10.2. This is especially relevant since the pion included in [8] is the lightest meson, hence pion systems are expected to have the largest relativistic correction.

11.1 Future studies

The examination of the explicit meson model so far leaves a number of possibilities for further examinations of the model. As mentioned in [5] the findings in [5] might indicate that the two-pion effect is not negligible. Hence, future studies can investigate photoproduction of neutral pions off protons in the two-pion approximation. In an investigation of this subject the results in [11] can be applied.

Another subject more directly linked to this thesis is the analysis of the deuteron with explicit pions. This subject can be expanded to include photoproduction off the deuteron. If the same coupling term is able to produce a reasonable ground state energy and charge radius for the deuteron and a cross section for pion photoproduction that repro-

duces the experimental findings, it will be a great success for the explicit meson model.

The explicit meson model can also be tested on more complex nuclei than the deuteron, examining the broader application of the model. The explicit meson model has not yet been computed with a high number of mesons included into the explicit meson model. This can potentially reveal further insight into the explicit meson model's strengths and limitations.

Existing studies of the explicit meson model [6], [1], [5], [8], [11] and this thesis use a simple phenomenological coupling operator. Future studies can investigate if this is the correct form of the coupling.

12

Conclusion

In this thesis the explicit meson model, as described by Fedorov and Jensen in [1][6], has been investigated by applying it to the deuteron in the simple one sigma-meson version of the model.

The explicit meson model has several potential advantages compared to established few-body nuclear models. One is that the explicit meson model has a lower number of model parameters. Another is that the explicit meson model includes few-body forces. The model also includes meson physics into the nucleon-nucleon interaction.

In [1], the explicit meson model in the one sigma-meson incarnation was applied to deuteron, with the coupling operator in Eq. (4.15). The model was able to produce a bound deuteron state with ground state energy and charge radius very close to the experimental expectations. This result was successfully recreated in this thesis.

In [6] the same model is examined, the only difference being the coupling operator taking the form in Eq. (4.14). In [6] the explicit meson model was able to produce a bound deuteron state. But the explicit meson model was unable to produce a state with ground state energy and charge radius satisfyingly close to the expectations. These results were also successfully recreated.

The interaction in Eq. (4.14) allows for the formation of bound nucleon-meson states. By including these states into the explicit meson model in [6], the model produces bound deuteron states with ground state energy and charge radius close to the experimental expectations. Hence, confirming the validity of the explicit meson model with the realistic coupling in Eq. (4.14). This has not previously been published.

The ground state energy for systems consisting of a single nucleon and given number of mesons, can give an estimate of the contribution from higher order approximations. This is shown in Figs. 10.4 and 10.5. For a meson with a mass roughly equal to the pion the second order contribution becomes lower than 4 %, and lower than 0.3 % for the third order contribution.

The explicit meson model has been applied using classical kinetic energy. Computing a deuteron system with relativistic kinetic energy allow the relativistic ground state energies to be compared to their classical counterpart. It turns out that the deuteron ground state energy and charge radius have significant different values for the relativistic kinetic energy compared to the classical. Hence, the relativistic kinetic energy should be used in further studies. The previously discussed result can be recreated with the relativistic kinetic energy by tuning the free-parameters in the coupling operator. A comparison between the classical and relativistic energy in the explicit meson model for the deuteron has not been published previously.

A

Permutations of particles

Permutation symmetries play an import role in physics with identical particles [12]. The introduction of permutations also allows for the simplification of the calculation of the matrix element for the relativistic kinetic energy in Chapter 7. This section follows from [13].

In a system of N particles there is $N!$ possible permutations. For a given permutation $\mathcal{P} = \begin{pmatrix} 1 & 2 & \cdots & N \\ p_1 & p_2 & \cdots & p_N \end{pmatrix}$ the corresponding permutation operator P transforms the single particle coordinates as $\vec{r}_i \rightarrow \vec{r}_{p_i}$. The matrix form of the permutation operator is given by:

$$(P_{\mathcal{P}})_{ij} = \delta_{j\, p_i} \quad \text{for} \quad i, j = 1, 2, \ldots, N, \tag{A.1}$$

where δ_{ij} is the Kronecker delta.

For a system there is $3! = 6$ possible permutations given by the matrices:

$$P_{\binom{123}{123}} = \begin{pmatrix} 1 & 0 & 0 \\ 0 & 1 & 0 \\ 0 & 0 & 1 \end{pmatrix}, \quad P_{\binom{123}{213}} = \begin{pmatrix} 0 & 1 & 0 \\ 1 & 0 & 0 \\ 0 & 0 & 1 \end{pmatrix},$$
$$P_{\binom{123}{321}} = \begin{pmatrix} 0 & 0 & 1 \\ 0 & 1 & 0 \\ 1 & 0 & 0 \end{pmatrix}, \quad P_{\binom{123}{132}} = \begin{pmatrix} 1 & 0 & 0 \\ 0 & 0 & 1 \\ 0 & 1 & 0 \end{pmatrix},$$
$$P_{\binom{123}{123}} = \begin{pmatrix} 1 & 0 & 0 \\ 0 & 1 & 0 \\ 0 & 0 & 1 \end{pmatrix}, \quad P_{\binom{123}{213}} = \begin{pmatrix} 0 & 1 & 0 \\ 1 & 0 & 0 \\ 0 & 0 & 1 \end{pmatrix}. \tag{A.2}$$

In the three-particle system the cyclic permutations are $P_{\binom{123}{231}}$, $P_{\binom{123}{312}}$ and $P_{\binom{123}{123}}$.

Note that if the particles do not share the same masses, the permutation operator should also be applied to the mass vector.

A.1 Permutation of the center of mass coordinates

In Chapter 3 a coordinate transformation is described, $\mathbf{r} \to \mathbf{x} = J\mathbf{r}$. Let $\mathbf{r}^{(k)}$ be coordinates under a cyclic permutation:

$$J\mathbf{r}^{(k)} \equiv J^{(k)}\mathbf{r} \equiv x^{(k)}. \tag{A.3}$$

A permutation operator can be constructed in the center of mass coordinates as:

$$\mathbf{x}^{(k)} = P^{(k)}\mathbf{x}, \quad P^{(k)} = J^{(k)}J^{-1}. \tag{A.4}$$

As an example relevant for the calculations in Chapter 7, for a three-particle system the cyclic permutation of the coordinates yields the corresponding transformations:

$$J^{(1)} = \begin{pmatrix} 0 & 1 & -1 \\ -1 & \frac{m_2}{m_2+m_3} & \frac{m_3}{m_2+m_3} \\ \frac{m_1}{m_1+m_2+m_3} & \frac{m_2}{m_1+m_2+m_3} & \frac{m_3}{m_1+m_2+m_3} \end{pmatrix},$$

$$J^{(2)} = \begin{pmatrix} -1 & 0 & 1 \\ \frac{m_1}{m_1+m_3} & -1 & \frac{m_3}{m_1+m_3} \\ \frac{m_1}{m_1+m_2+m_3} & \frac{m_2}{m_1+m_2+m_3} & \frac{m_3}{m_1+m_2+m_3} \end{pmatrix},$$

$$J^{(3)} = J. \tag{A.5}$$

In Chapter 7 the application of the cyclic permutation operator is applied to calculate the matrix element for the relativistic kinetic energy.

B

Supplementary figures and tables

This chapter will feature a number of supplementary figures and tables to the main thesis. The data will be presented mostly without comments. The relevant information will be presented in form of notes. This will hopefully make it easy for the reader to find and interpretate the desired information.

B.1 Supplementary figures: Section 10.2.1

In Fig. B.1 the figure in Fig. 10.4 is recreated with constant coupling operator, as opposed to the mass dependent coupling in Fig. 10.4.

B.2 Supplementary figures: Section 10.2.2

This section features supplementary figures and tables to Section 10.2.2. The convergence is shown in Figs. B.2 to B.4. In Table B.1 an example of the tuned model is shown.

B.3 Supplementary figures to Section 10.3

This section features Fig. B.5 which depict the charge radius component of Fig. 10.7.

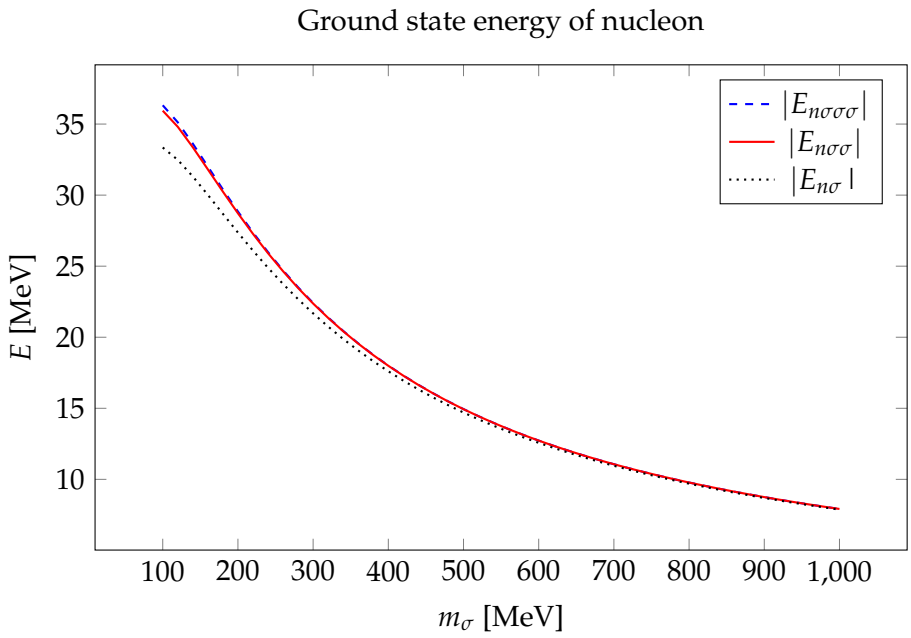

Figure B.1: Ground state energy of nucleon with constant coupling. Systems: nucleon-meson (with energy $E_{n\sigma}$), nucleon-meson-meson (with energy $E_{n\sigma\sigma}$) and nucleon-meson-meson-meson (with energy $E_{n\sigma\sigma\sigma}$). Meson mass: m_σ. Coupling: Eq. (4.14). Number of allowed mesons: one to three. Strength parameter: $g = 77.5\,\text{MeV}$. Range parameter: $\gamma = 2.09\,\text{fm}$. Number of two-body Gaussians: $n_{(2)} = 14$. Number of three-body Gaussians: $n_{(3)} = 80$. Number of four-body Gaussians: $n_{(4)} = 100$. Kinetic energy: classical.

$n_{(2)}$	$n_{(3)}$	$n_{(4)}$	g	γ	V	R_c	E_0
9	50	100	62.9 MeV	2.41 fm	0.0017	2.13 fm	−2.23 MeV

Table B.1: Tuned model in the two-meson approximation. Systems: deuteron with dressed nucleons. Meson mass: $m_\sigma = 500\,\text{MeV}$. Coupling: Eq. (4.14). Number of allowed mesons: two. Strength parameter: g. Range parameter: γ. Number of two-body Gaussians: $n_{(2)}$. Number of three-body Gaussians: $n_{(3)}$. Number of four-body Gaussians: $n_{(4)}$. Kinetic energy: classical. Root square sum of relative errors: V.

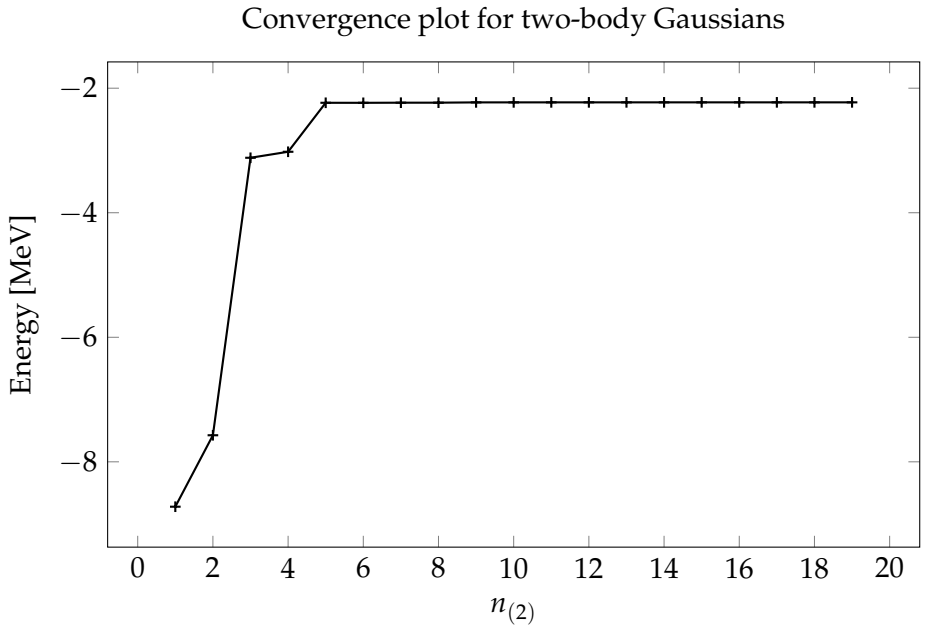

Figure B.2: Convergence plot for two-body Gaussians. Systems: deuteron with dressed nucleons. Meson mass: $m_\sigma = 500\,\text{MeV}$. Coupling: Eq. (4.14). Number of allowed mesons: two. Strength parameter: $g = 62.9\,\text{MeV}$. Range parameter: $\gamma = 2.41\,\text{fm}$. Number of two-body Gaussians: $n_{(2)}$. Number of three-body Gaussians: $n_{(3)} = 50$. Number of four-body Gaussians: $n_{(4)} = 100$. Kinetic energy: classical.

B.4 Recreation of results from Section 9.1 with relativistic energy

In this section the results in Section 9.1 are recreated using relativistic kinetic energy.

In Table B.2 an example of the tuned model is shown. Figs. B.6 to B.8 are the recreation of Figs. 9.1 to 9.3 respectively with relativistic kinetic energy.

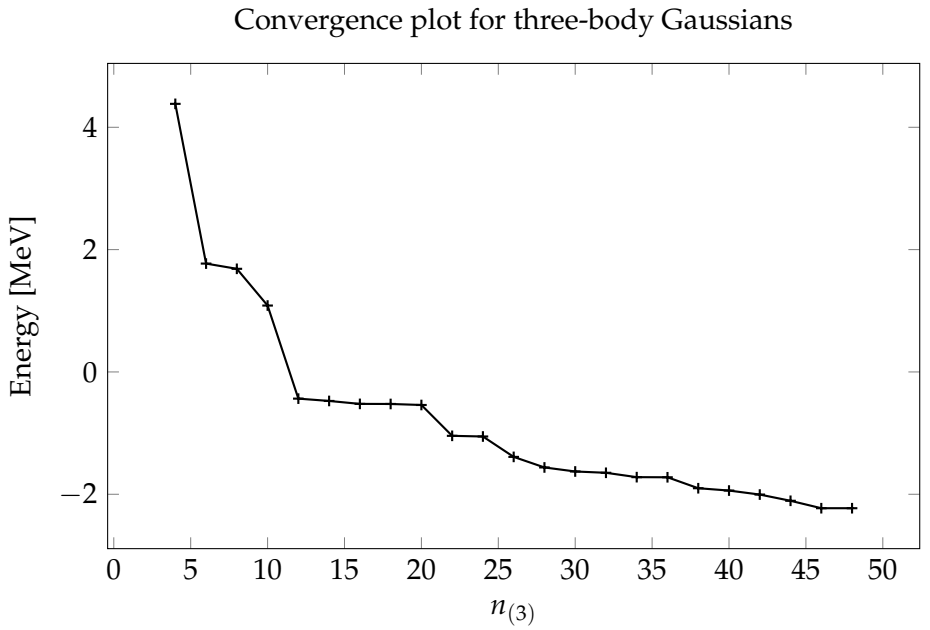

Figure B.3: Convergence plot for three-body Gaussians. Systems: deuteron with dressed nucleons. Meson mass: $m_\sigma = 500\,\text{MeV}$. Coupling: Eq. (4.14). Number of allowed mesons: two. Strength parameter: $g = 62.9\,\text{MeV}$. Range parameter: $\gamma = 2.41\,\text{fm}$. Number of two-body Gaussians: $n_{(2)}$. Number of three-body Gaussians: $n_{(3)}$. Number of four-body Gaussians: $n_{(4)} = 100$. Kinetic energy: classical.

$n_{(2)}$	$n_{(3)}$	S_σ	b_σ	V	R_c	E_0
10	50	17.3 MeV	3.19 fm	4.47×10^{-6}	2.13 fm	−2.22 MeV

Table B.2: Recreation of results from Section 9.1 with relativistic energy. Systems: deuteron. Meson mass: $m_\sigma = 500\,\text{MeV}$. Coupling: Eq. (4.15). Number of allowed mesons: one. Strength parameter: S_σ. Range parameter: b_σ. Number of two-body Gaussians: $n_{(2)}$. Number of three-body Gaussians: $n_{(3)}$. Kinetic energy: relativistic. Root square sum of relative errors: V.

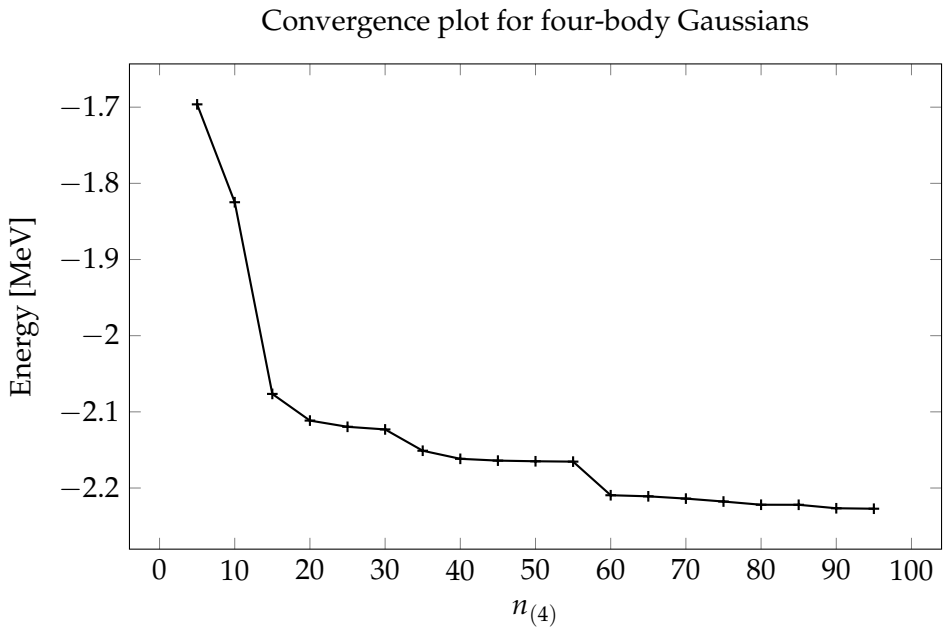

Figure B.4: Convergence plot for four-body Gaussians. Systems: deuteron with dressed nucleons. Meson mass: $m_\sigma = 500\,\text{MeV}$. Coupling: Eq. (4.14). Number of allowed mesons: two. Strength parameter: $g = 62.9\,\text{MeV}$. Range parameter: $\gamma = 2.41\,\text{fm}$. Number of two-body Gaussians: $n_{(2)} = 9$. Number of three-body Gaussians: $n_{(3)} = 50$. Number of four-body Gaussians: $n_{(4)}$. Kinetic energy: classical.

B.5 Recreation of results from Section 9.2 with relativistic energy

In this section the results in Section 9.2 are recreated using relativistic kinetic energy.

In Table B.3 an example of the tuned model is shown. Figs. B.9 and B.10 are the recreation of Figs. 9.4 and 9.5 respectively with relativistic kinetic energy.

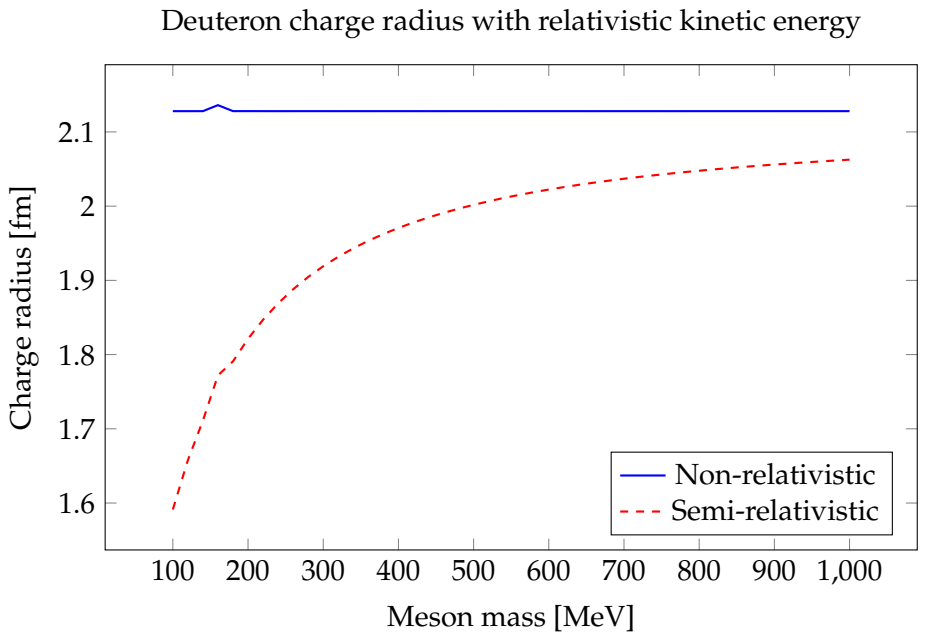

Figure B.5: Deuteron charge radius with relativistic kinetic energy. Systems: deuteron. Meson mass: m_σ. Coupling: Eq. (4.15). Number of allowed mesons: one. Strength parameter: variable. Range parameter: variable. Number of two-body Gaussians: $n_{(2)} = 6$. Number of three-body Gaussians: $n_{(3)} = 52$.

$n_{(2)}$	$n_{(3)}$	g	γ	V	R_c	E_0
10	50	37.8 MeV	2.09 fm	0.942	4.03 fm	−2.88 MeV

Table B.3: Recreation of results from Section 9.2 with relativistic energy. Systems: deuteron. Meson mass: $m_\sigma = 500\,\text{MeV}$. Coupling: Eq. (4.14). Number of allowed mesons: one. Strength parameter: g. Range parameter: γ. Number of two-body Gaussians: $n_{(2)}$. Number of three-body Gaussians: $n_{(3)}$. Kinetic energy: relativistic. Root square sum of relative errors: V.

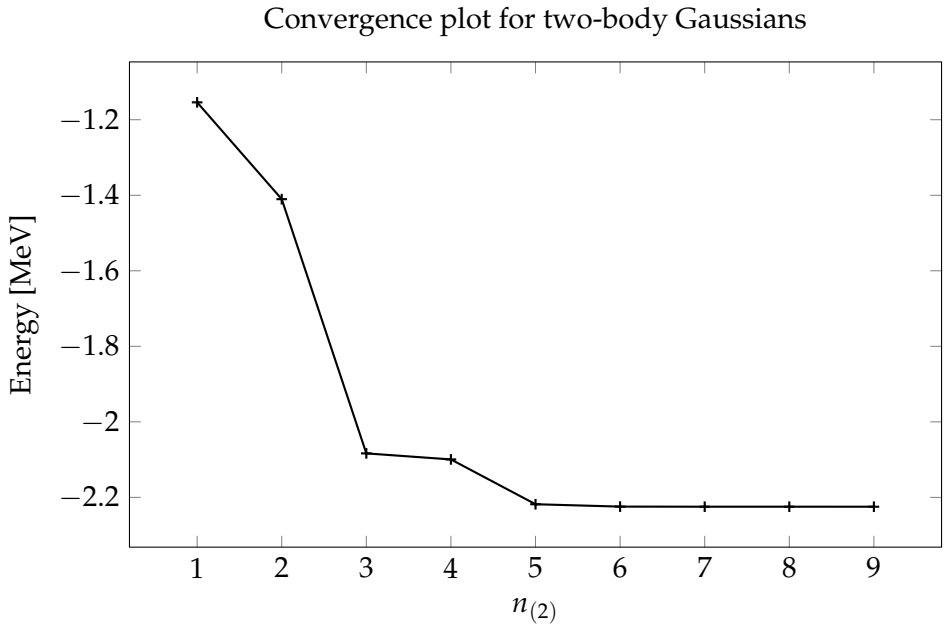

Figure B.6: Convergence plot for two-body Gaussians. Recreation of Fig. 9.1 with relativistic energy. Systems: deuteron. Meson mass: $m_\sigma = 500\,\text{MeV}$. Coupling: Eq. (4.15). Number of allowed mesons: one. Strength parameter: $S_\sigma = 17.3\,\text{MeV}$. Range parameter: $b_\sigma = 3.19\,\text{fm}$. Number of two-body Gaussians: $n_{(2)}$. Number of three-body Gaussians: $n_{(3)} = 50$. Kinetic energy: relativistic.

B.6 Recreation of results from Section 10.1 with relativistic energy

In this section the results in Section 10.1 are recreated using relativistic kinetic energy.

In Table B.4 an example of the tuned model is shown. Figs. B.11 to B.13 are the recreation of Figs. 10.1 to 10.3 respectively with relativistic kinetic energy.

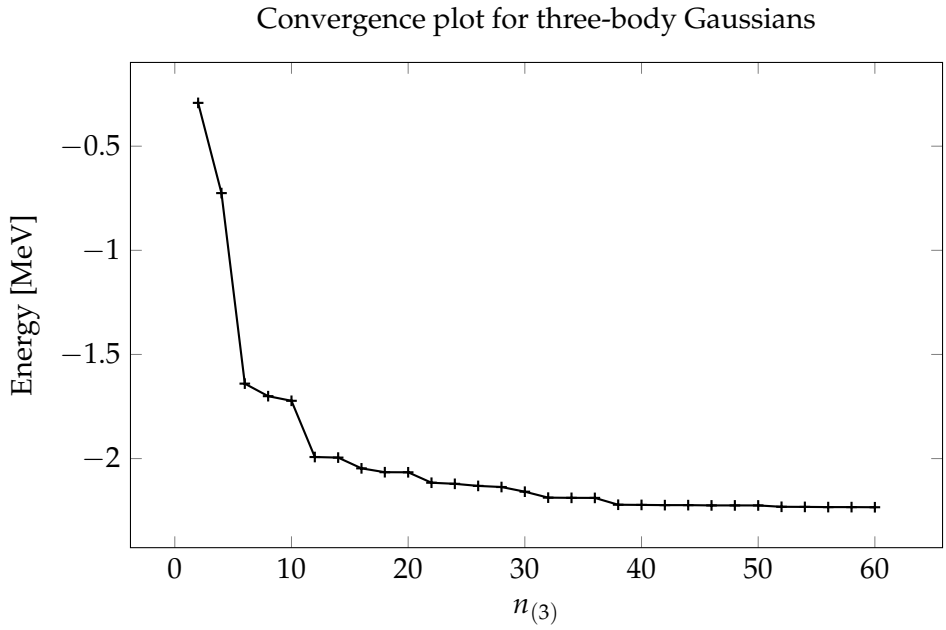

Figure B.7: Convergence plot for three-body Gaussians. Recreation of Fig. 9.2 with relativistic energy. Systems: deuteron. Meson mass: $m_\sigma = 500\,\text{MeV}$. Coupling: Eq. (4.15). Number of allowed mesons: one. Strength parameter: $S_\sigma = 17.3\,\text{MeV}$. Range parameter: $b\sigma = 3.19\,\text{fm}$. Number of two-body Gaussians: $n_{(2)} = 10$. Number of three-body Gaussians: $n_{(3)}$. Kinetic energy: relativistic.

$n_{(2)}$	$n_{(3)}$	g	γ	V	R_c	E_0
10	50	62.5 MeV	2.40 fm	2.67×10^{-6}	2.13 fm	−2.23 MeV

Table B.4: Recreation of results from Section 10.1 with relativistic energy. Systems: deuteron with dressed nucleons. Meson mass: $m_\sigma = 500\,\text{MeV}$. Coupling: Eq. (4.14). Number of allowed mesons: one. Strength parameter: g. Range parameter: γ. Number of two-body Gaussians: $n_{(2)}$. Number of three-body Gaussians: $n_{(3)}$. Kinetic energy: relativistic. Root square sum of relative errors: V.

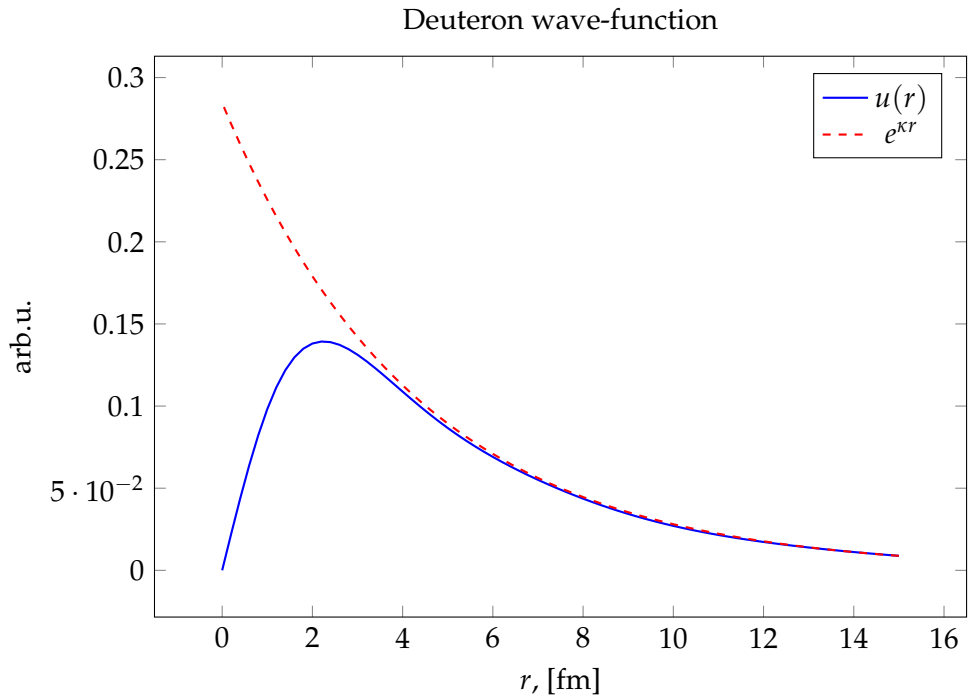

Figure B.8: Deuteron wave-function. Recreation of Fig. 9.3 with relativistic energy. Systems: deuteron. Meson mass: $m_\sigma = 500\,\text{MeV}$. Coupling: Eq. (4.15). Number of allowed mesons: one. Strength parameter: $S_\sigma = 17.3\,\text{MeV}$. Range parameter: $b_\sigma = 3.19\,\text{fm}$. Number of two-body Gaussians: $n_{(2)} = 10$. Number of three-body Gaussians: $n_{(3)} = 50$. Kinetic energy: relativistic.

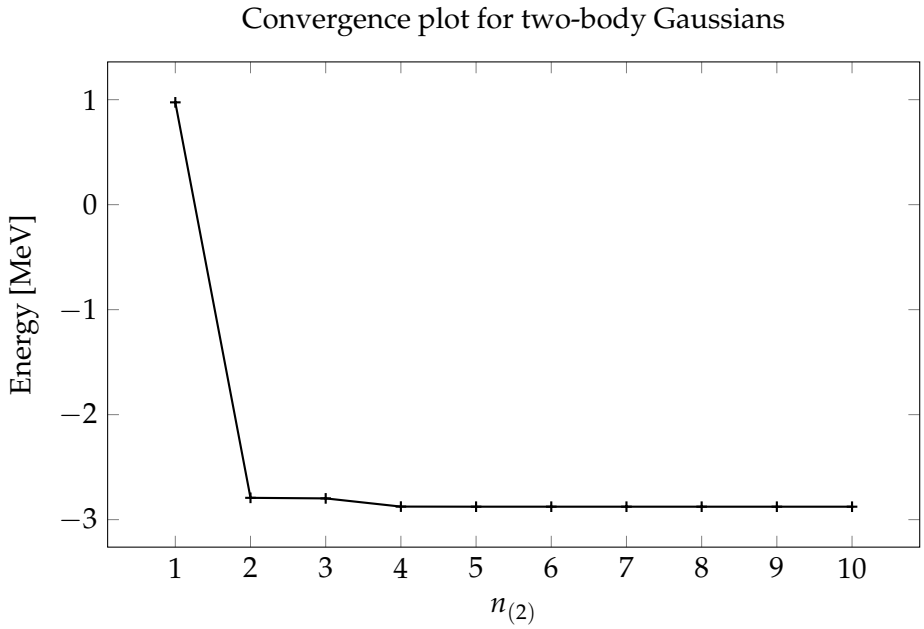

Figure B.9: Convergence plot for two-body Gaussians. Recreattion of Fig. 9.4 with relativistic energy. Systems: deuteron. Meson mass: $m_\sigma = 500\,\text{MeV}$. Coupling: Eq. (4.14). Number of allowed mesons: one. Strength parameter: $g = 37.8\,\text{MeV}$. Range parameter: $\gamma = 2.09\,\text{fm}$. Number of two-body Gaussians: $n_{(2)}$. Number of three-body Gaussians: $n_{(3)} = 50$. Kinetic energy: relativistic.

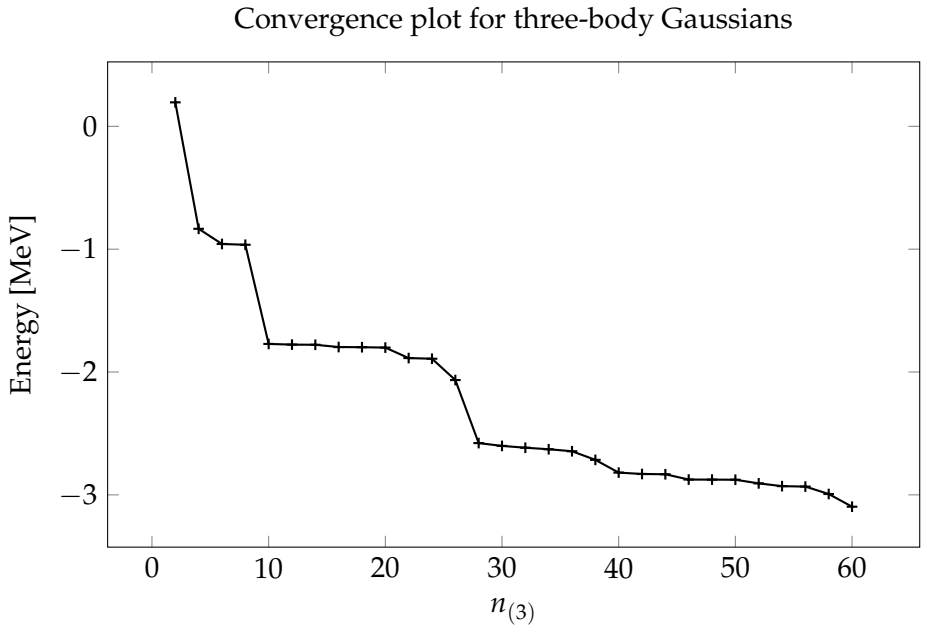

Figure B.10: Convergence plot for three-body Gaussians. Recreation of Fig. 9.5 with relativistic energy. Systems: deuteron. Meson mass: $m_\sigma = 500\,\text{MeV}$. Coupling: Eq. (4.14). Number of allowed mesons: one. Strength parameter: $g = 37.8\,\text{MeV}$. Range parameter: $\gamma = 2.09\,\text{fm}$. Number of two-body Gaussians: $n_{(2)} = 10$. Number of three-body Gaussians: $n_{(3)}$. Kinetic energy: relativistic.

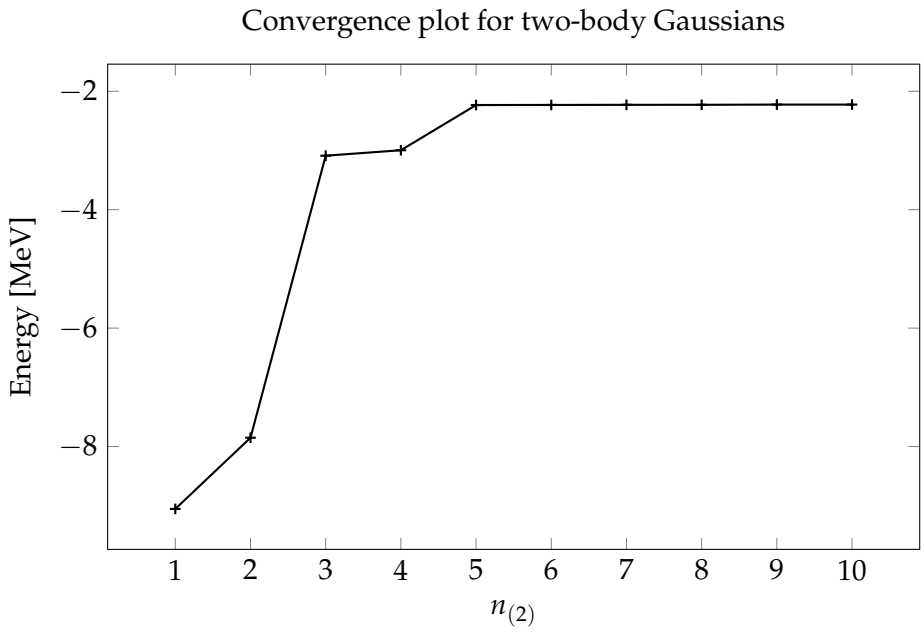

Figure B.11: Convergence plot for two-body Gaussians. Recreation of Fig. 10.1 with relativistic energy. Systems: deuteron with dressed nucleons. Meson mass: $m_\sigma = 500\,\text{MeV}$. Coupling: Eq. (4.14). Number of allowed mesons: one. Strength parameter: $g = 62.5\,\text{MeV}$. Range parameter: $\gamma = 2.40\,\text{fm}$. Number of two-body Gaussians: $n_{(2)}$. Number of three-body Gaussians: $n_{(3)} = 50$. Kinetic energy: relativistic.

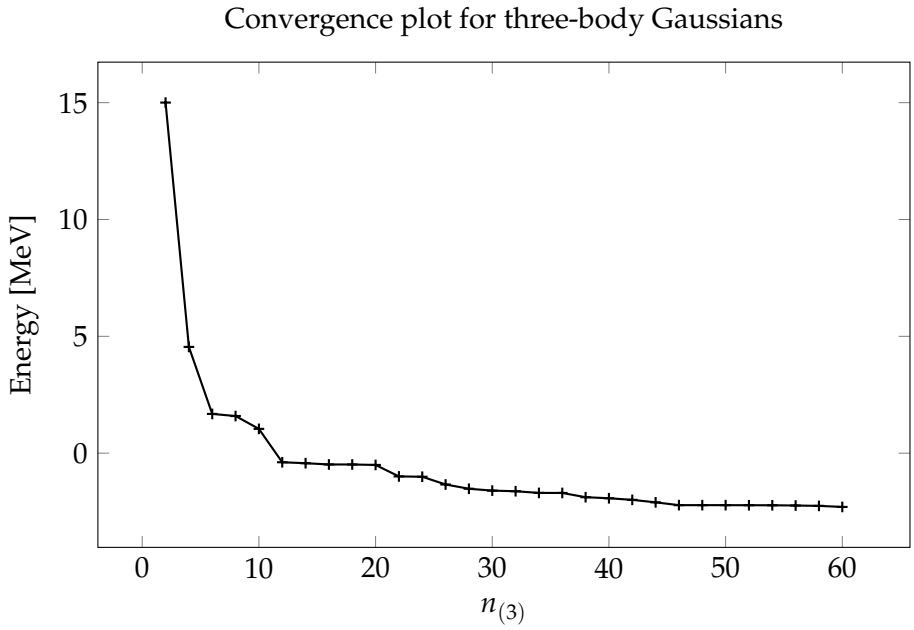

Figure B.12: Convergence plot for three-body Gaussians. Recreation of Fig. 10.2 with relativistic energy. Systems: deuteron with dressed nucleons. Meson mass: $m_\sigma = 500\,\text{MeV}$. Coupling: Eq. (4.14). Number of allowed mesons: one. Strength parameter: $g = 62.5\,\text{MeV}$. Range parameter: $\gamma = 2.40\,\text{fm}$. Number of two-body Gaussians: $n_{(2)}$. Number of three-body Gaussians: $n_{(3)} = 50$. Kinetic energy: relativistic.

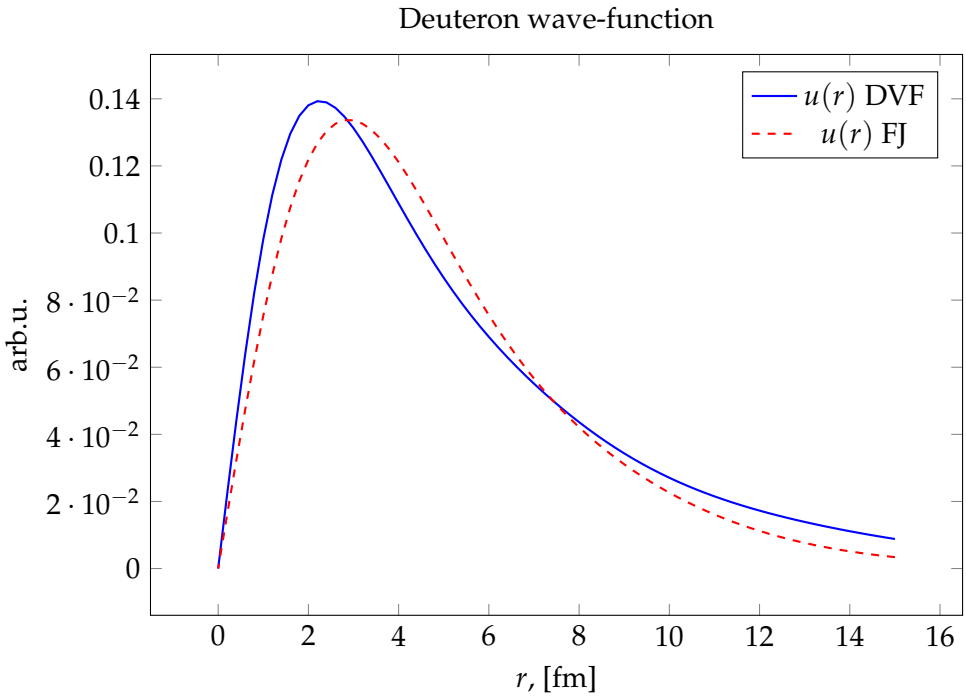

Figure B.13: Deuteron wave-function. Recreation of Fig. 10.3 with relativistic energy. Systems: deuteron with dressed nucleons. Meson mass: $m_\sigma = 500\,\text{MeV}$. Coupling: Eq. (4.14). Number of allowed mesons: one. Strength parameter: $g = 62.5\,\text{MeV}$. Range parameter: $\gamma = 2.40\,\text{fm}$. Number of two-body Gaussians: $n_{(2)} = 10$. Number of three-body Gaussians: $n_{(3)} = 50$. Kinetic energy: relativistic.

Bibliography

[1] D. V. Fedorov. "A Nuclear Model with Explicit Mesons". In: *Few-Body Systems* 61.4 (Oct. 2020). DOI: 10.1007/s00601-020-01573-1. URL: https://doi.org/10.1007%2Fs00601-020-01573-1.

[2] D. V. Fedorov. "Analytic Matrix Elements and Gradients with Shifted Correlated Gaussians". In: *Few-Body Systems* 58.1 (Dec. 2016). DOI: 10.1007/s00601-016-1183-0. URL: https://doi.org/10.1007%2Fs00601-016-1183-0.

[3] D. V. Fedorov. "Correlated Gaussians and Low-Discrepancy Sequences". In: *Few-Body Systems* 60.3 (2019). DOI: 10.1007/s00601-019-1521-0. URL: https://doi.org/10.1007%2Fs00601-019-1521-0.

[4] D. V. Fedorov. "Yet Another Introduction to Numerical Methods version 20.05". Lecture Notes. 2020.

[5] D. V. Fedorov and M. Mikkelsen. "Threshold Photoproduction of Neutral Pions Off Protons in Nuclear Model with Explicit Mesons". In: *Few-Body Systems* 64.1 (Dec. 2022). DOI: 10.1007/s00601-022-01783-9. URL: https://doi.org/10.1007%2Fs00601-022-01783-9.

[6] Filip Jensen. "Nuclear Interaction Model with Explicit Mesons". MA thesis. Aarhus University, May 2019.

[7] B. R. Martin. *Nuclear and Particle Physics*. John Wiley and Sons, Ltd, July 2006.

[8] Martin Mikkelsen. "Threshold Pion Photoproduction off Nucleons using the Nuclear Model with Explicit Pions". MA thesis. Aarhus University, Nov. 2022.

[9] Peter J. Mohr, David B. Newell, and Barry N. Taylor. "CODATA recommended values of the fundamental physical constants: 2014". In: *Reviews of Modern Physics* 88.3 (Sept. 2016). DOI: 10.1103/revmodphys.88.035009. URL: https://doi.org/10.1103%2Frevmodphys.88.035009.

[10] John A. Nelder and Roger Mead. "A Simplex Method for Function Minimization". In: *Comput. J.* 7 (1965), pp. 308–313.

[11] Martin Cradock Østerlund. "Dressing of Proton with Virtual Pions in a Nuclear Model with Explicit Mesons". MA thesis. Aarhus University, June 2022.

[12] J. J. Sakurai and Jim Napolitano. *Modern Quantum Mechanics*. Second. Cambridge University Press, 2017.

[13] Yasuyuki Suzuki and Kálmán Varga. *Stochastic Variational Approach to Quantum-Mechanical Few-Body Problems*. Springer, 1998.

[14] Vladimir Zelevinsky and Alexander Volya. *Physics of Atomic Nuclei*. Wiley-VCH, 2017.